MASARYKOVA UNIVERZITA
PŘÍRODOVĚDECKÁ FAKULTA
ÚSTAV TEORETICKÉ FYZIKY A ASTROFYZIKY

Bakalářská práce

BRNO 2012   **MICHAL PRIŠEGEN**

MASARYKOVA UNIVERZITA
PŘÍRODOVĚDECKÁ FAKULTA
ÚSTAV TEORETICKÉ FYZIKY A ASTROFYZIKY

Studium rentgenových dvojhvězd s hmotnou složkou

Bakalářská práce

Michal Prišegen

Vedoucí práce: Mgr. Filip Hroch, Ph.D.   **Brno 2012**

Bibliografický záznam

Bibliographic Entry

Abstrakt

Tato bakalářská práce se zabývá studiem rentgenových dvojhvězd s hmotnou složkou (neboli HMXBs z jejich anglického názvu High Mass X-Ray Binaries) pomocí takzvaných stelárních rázových vln. Ty se často utvářejí u objektů s vysokou rychlostí vůči okolnímu prostředí a poskytují informace o pohybu hvězdy, hvězdném větru a okolním mezihvězdném prostředí. U HMXB systémů jsou však poměrně vzácné. Jádrem této práce je infračervená prohlídka všech známých HMXB systémů a HMXB kandidátů zaměřená na detekci těchto útvarů. Výsledkem prohlídky je objev dvou nových rázových vln spojených s HMXB. V další části práce pak diskutujeme vlastnosti dohromady čtyř HMXB systémů s rázovými vlnami, zejména strukturu a spektrum rázových vln, korelaci mezi pohybem systémů odvozených z geometrie rázových vln a z astrometrie, možné místa zrodu HMXB systémů, zbytky supernov s nima spojené a vlastnosti okolního mezihvězdného prostředí.

Abstract

This bachelor thesis focuses on studying High Mass X-ray binaries (HMXBs) via stellar bow shocks. These frequently form around objects possessing high velocities with respect to the local ambient medium, providing us with the information on the system's movement, stellar wind and properties of the surrounding interstellar medium. However, bow shocks associated with HMXBs are relatively rare. The core of this work is the infrared bow shock survey of all HMXBs and HMXB candidates. The result is a discovery of two new bow shocks associated with a HMXB. We then discuss various properties of altogether four HMXB systems with bow shocks, mainly the structure and spectrum of the bow shocks, the correlation between the velocities inferred from the bow shock geometry and proper motion measurements, possible formation sites and supernova remnants associated with the systems and the properties of the surrounding interstellar medium.

Masarykova univerzita

Přírodovědecká fakulta

ZADÁNÍ BAKALÁŘSKÉ PRÁCE

Student : **Michal Prišegen**
Studijní program : **Aplikovaná fyzika**
Studijní obor : **Astrofyzika**

Ředitel Ústavu teoretické fyziky a astrofyziky PřF MU Vám ve smyslu Studijního a zkušebního řádu MU určuje bakalářskou práci s tématem:

Studium rentgenových dvojhvězd s hmotnou složkou

Study of high-mass X-ray binaries

Zásady pro vypracování:
Rentgenové dvojhvězdy s hmotnou složkou, v angličtině high-mass X-ray binaries (HMXB), jsou dvojhvězdy jejíž jednou složkou je kompaktní objekt (bílý trpaslík, neutronová hvězda nebo černá díra) a druhou složkou hmotná horká hvězda, jejíž hvězdný vítr je zachytáván kompaktní složkou. Přitom je emitováno velké množství rentgenova záření. Cílem této práce je studium observačních projevů vhodných HMXB za pomocí dostupných optických dat stejně jako dat z kosmických sond. Pro úspěšné vypracování se předpokládá znalost základů astronomické fotometrie a spektroskopie a příslušných fyzikálních partií. Práce bude vypracována v angličtině.

Vedoucí bakalářské práce : Mgr. Filip Hroch, Ph.D.
Datum zadání bakalářské práce : září 2011
Datum odevzdání bakalářské práce : dle harmonogramu ak. roku 2011/2012

V Brně dne 13. 12. 2011

Prof. Rikard von Unge, Ph.D.
ředitel Ústavu teoretické fyziky a astrofyziky
PřF MU

Zadání bakalářské práce převzal dne:

Podpis studenta

14.12.2011

Poděkování

Chcel by som sa poďakovať vedúcemu mojej bakalárskej práce Filipovi Hrochovi za jeho trpezlivosť a všetky cenné rady, ktoré mi neváhal poskytnúť kedykoľvek, keď som to potreboval.

Prohlášení

Prohlašuji, že jsem svoji bakalářskou/diplomovou/rigorózní práci vypracoval samostatně█ s využitím informačních zdrojů, které jsou v práci citovány.

Brno 21. května 2012 . . . .
Michal Prišegen

Contents

Chapter 1

Introduction

Astronomy, arguably the oldest branch of science, amazed the mankind from the dawn of ages. Serving many vital everyday purposes, astronomy also fueled many philosophical debates. The invention of the telescope and its subsequent utilization for astronomy brought forth the era of astrophysics as the heavens unveiled many of its secrets, hidden to the naked eye. However, the work of an astronomer remained practically unchanged, observing the sky 'till the stars fade away'. The major metamorphosis of the subject was yet to happen. It came to pass with the employment of photographic and spectroscopic techniques and later, in the previous century, with opening the radio window and launching satellites to observe the sky in various spectral bands. Indeed, our ventures above the Earth's atmosphere, the advances in radio astronomy and, last but not least, our progress in technology opened up new vistas onto the Universe. This work will focus on High Mass X-ray Binaries – just one of many types of exotic objects recently discovered and extremely interesting to study in all spectral bands.

1.1   A brief history

The history of research into High Mass X-ray Binaries (HMXBs) spans only a few decades. It all started when Giacconi et al.[1] launched an Aerobee rocket, discovering Scorpius X-1 (abbreviated Sco X-1, according to naming nomenclature indicating that it was the first X-ray source discovered in that particular constellation), the first extrasolar X-ray source and, in fact, the strongest source of X-rays in the sky (in the energy band 1 – 10 keV). Other discoveries of discrete X-ray sources soon followed as many more observations using balloons and rockets were carried out, confirming the initial observations and refining the old ones. By the end of the sixties about 20 X-ray sources had been confirmed and one of them – Cygnus X-1, in fact a HMXB, was found to vary in time.

There has been a lot of effort to explain the nature of these newly discovered mysterious sources. In 1965, Zel'dovich and Guseynov[2] came up with an idea that the discovery of X-ray or gamma ray radiation emitted from a single-line spectroscopic binary (single-line means that spectral lines from only one object are detectable) provides evidence of the presence of a neutron star or a black hole in the system as neither of these objects can produce optical spectral lines. The first interesting theory explaining the underlying mechanisms producing X-ray radiation was proposed by Shklovskii[3] for Sco X-1, where
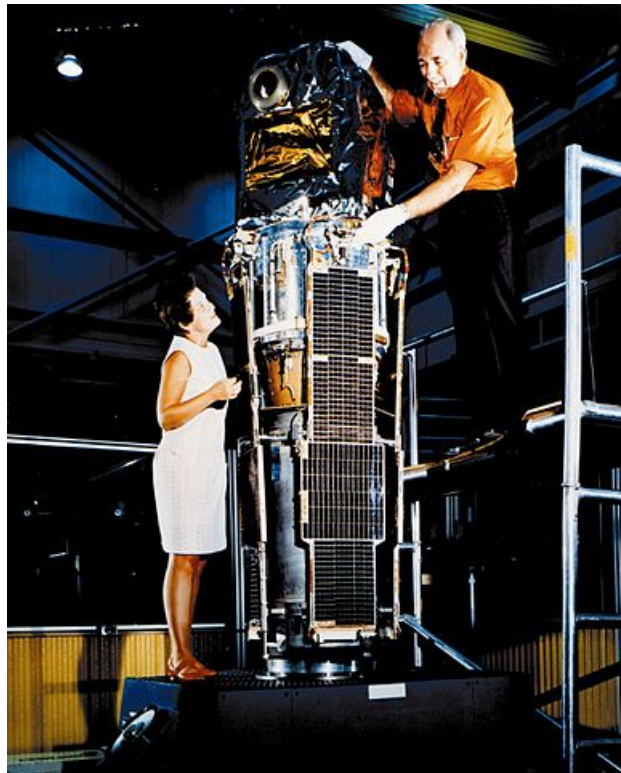
Figure 1.1: Uhuru, the first dedicated X-ray satellite. Courtesy of NASA

they adopted and slightly altered the original idea from Hayakawa and Matsuoka (1964) for different kinds of systems. The concept was that the X-ray emission originates from high-temperature gas flowing onto a neutron star from a close binary companion. This theory, quite radical for that time, was subjected to close scientific scrutiny. In 1968, Prendergast and Burbidge[4] argued that it was not possible for gas falling onto a compact object to flow radially as it would have too much orbital angular momentum to do so. Instead, they proposed a model where the gas forms a thin accretion disc around the compact star, while the gas will have a small inward drift velocity as well.

Despite of the relative feasibility of rocket and baloon observations, there were inherent limitations to this kind of observation techniques – mainly the limited amount of time during which the data could be acquired. The observations needed to be taken to space. The first satellite dedicated entirely to the study of the cosmic X-ray sources, Uhuru ('freedom' in Swahili), was launched in 1970. It greatly expanded our knowledge of discrete X-ray sources, identifying over 300 of them and producing an extensive catalogue of them; its final version is known as the 4U Catalogue, containing many HMXBs.

The great success of the Uhuru mission paved the way for ten more missions in the seventies and to many more in the following decades. As of February 1, 2008 in the latest 4th edition of Catalogue of High Mass X-ray binaries in the Galaxy[5], there are 114 HMXB candidates. Moreover, the number of HMXBs in external galaxies is also rapidly increasing. Nowadays, HMXBs are subject of interest to many satellite X-ray observatories including XMM–Newton (low to mid energy X-rays 0.1 – 15 keV), INTEGRAL (high energy X-rays 15 – 60 keV), Swift and Chandra. However, as they are interesting to study

in various spectral bands, they are frequently observed by other space observatories, most notably the Hubble Space Telescope (HST) or Spitzer Infrared Telescope and by many ground base radio and optical telescopes as well.

1.2 The overview of X-ray binaries
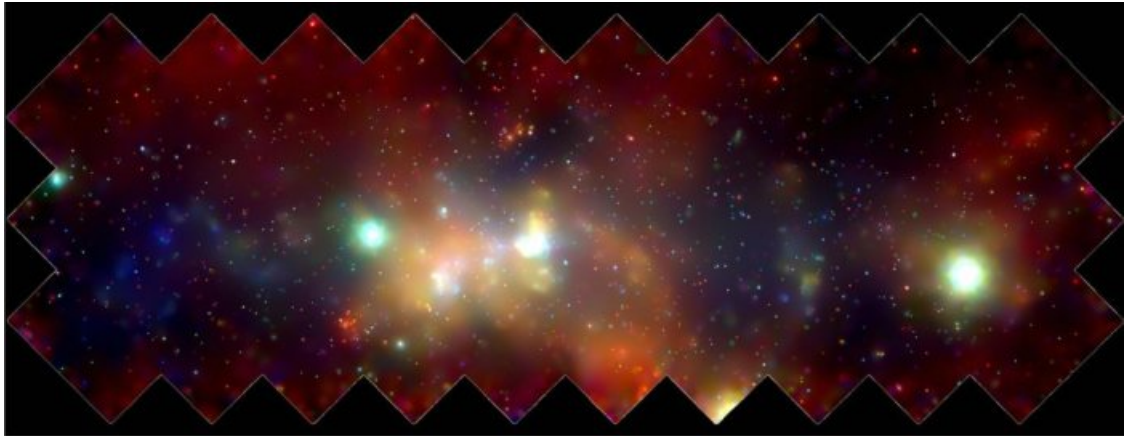
Figure 1.2: Chandra image of the Milky way. The small point source are predominantly X-ray binaries in our own galaxy. Image courtesy Chandra

As previously mentioned, X-ray binaries are the brightest X-ray sources in the sky. These binary systems contain a compact object which is either a white dwarf, a neutron star or a black hole (the primary component) and a normal star which is in the process of stellar evolution (the secondary component), revolving around their common center of mass[6]. The compact primary component accretes matter from the secondary star, either by capturing matter from its stellar wind or by direct mass transfer through the inner Lagrangian point from the surface of the secondary if the star has filled its Roche lobe (the process is called Roche-lobe overflow). Due to angular-momentum conservation, the matter accreting onto the primary settles in an accretion disk where viscous stresses heat the matter to extreme temperatures. At temperatures this high, the accretion disc radiates primarily in X-rays, hence giving this class of objects its name (In addition to the thermal X-ray emission from the accretion disk, X-ray binaries often also emit a power-law spectrum of hard X-rays and even gamma-rays.)[7] .

Depending on the mass of the secondary star, we classify these systems into two main types: Low Mass X-ray Binaries (LMXBs; mass of the secondary $\leq 3M_\odot$) and High Mass X-ray binaries (HMXBs; mass of the secondary $\geq 10M_\odot$). The HMXBs contain massive and early type (spectral class O or B) companions whereas in the case of LMXBs, the spectral type of the binary companion is A or later. In spite of the fact that both groups emit in X-rays, they differ from one another significantly[6].

The main discerning feature (which also leads to various additional effects) in these two types of objects is the way they capture the material from the secondary. The manner in which a compact object can accrete matter from its companion depends mostly on the mode of mass transfer, the ratio of the masses of the primary compact object and the secondary

Figure 1.3: Classification of X-ray binaries, (Reig)[14]

star, and their orbital separation. For instance, if the primary is a neutron star, a stable mass transfer through the inner Lagrangian point occurs only when the secondary has filled its Roche lobe and its mass is smaller than that of the neutron star. In these systems, mass is driven by angul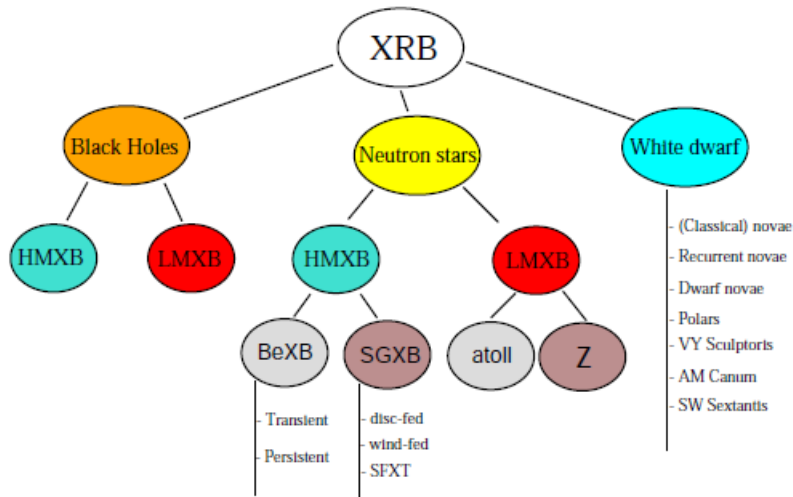ar momentum losses due to the gravitational radiation (for very small masses and orbital separations), magnetic braking (for periods shorter than 2 days) or by the evolution of the companion star (systems with longer orbital periods). The brightness of the system in the optical wavelenghts is much less than its brightness in the X-rays. This is the case with LMXBs - binary systems with low-mass companions to the neutron stars or black holes. The primary can also accrete matter from a companion that does not fill its Roche lobe, if the secondary is loosing matter in the form of a stellar wind. At the first glance this process might appear inefficient. To produce a bright X-ray source, the companion star must be very massive in order to drive a sufficient wind, loosing a considerable amount of matter. In this configuration, the massive, bright secondary dominates the system; its optical luminosity comprises the major portion of the total emission of the system. The rate of mass transfer is determined by the strength and speed of the stellar wind and the orbital separation of the system. Such systems are classified as HMXBs. There are some cases when a HMXB accretes the matter through the Roche-lobe overflow, however, the dominant process is still the capture of the stellar wind of the companion.

The different masses of the secondary stellar components of LMXBs and HMXBs have additional ramifications for these systems. It is a well-known astrophysical fact that the stars with different masses have different lifespans. Thus the lifetimes of HMXBs are dictated by the evolution of their massive stellar secondaries and are relatively short ($\sim 10^5 - 10^7$ years), whereas the lifetimes of LMXBs are determined predominantly by the mass-transfer processes and thus are longer ($\sim 10^7 - 10^9$ years). LMXBs can then travel further away from their place of birth. For this reason, LMXBs are found primarily near the galactic center and in the globular clusters, whereas HMXBs are distributed along the galactic plane, as young stellar populations are, unable to float too far away from them. In addition to this, because of their shorter lifespan, neutron stars in HMXBs accrete matter
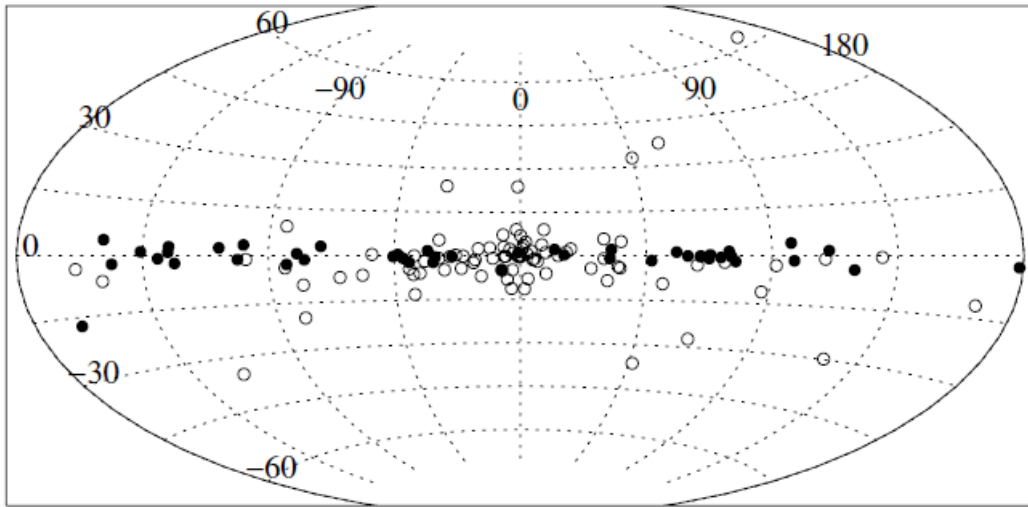
Figure 1.4: Distribution of Low Mass X-ray binaries (open symbols) and High Mass X-ray binaries (filled symbols) in galactic coordinates (Grimm et al. 2002)

for a relatively short time, so their magnetic fields do not decrease significantly from their high initial values. These stars appear as a accretion-powered pulsars. On the other side, in the case of LMXBs, the prolonged accretion onto the primary is responsible for the dampening of the magnetic fields and the absence of periodic pulsations in almost all cases. LMXBs also tend to have softer spectra (they emit lower energy X-rays), whereas HMXBs have harder spectra (higher energy X-rays).

HMXB	LMXB
Optical counterpart is a massive and luminous early-type star, O or early B	Faint blue optical counteparts
Concentrated in the galactic plane; young stellar population, age $< 10^7$ yr	Concentrated towards the galactic centre; fairly widespread around the galactic plane; old stellar population; age $(5-15) \times 10^9$ yr
Regular X-ray pulsations; no X-ray outbursts	X-ray outbursts; regular X-ray pulsations only in a few cases
Relatively hard X-ray spectra with $k_B T > 15$ keV	Softer X-ray spectra; with $k_B T < 10$ keV

Table 1.1: The summary of the main differences between the two main types of X-ray binaries

It is estimated that they are only a few hundred X-ray binaries in our Galaxy, making them an extreme rarity among stellar systems. The original binary must follow a large number of improbable evolutionary steps in a precise order to become an X-ray source. Moreover, the supernova explosions, essential for the formation of an X-ray binary and

preceding the formation of the compact objects may break up the binary just prior to becoming an X-ray source.[8],[9],[10]

1.3 Motivation

There is no doubt that the study of binary stars brought about major breakthroughs in the field of astrophysics. It is quite fortunate that the stars come in pairs so often as we are able to learn much more about them. Indeed, the wealth of information that we are able to extract from a binary is far greater than the amount of information obtainable from a solitary star. In addition to this, the existing research into HMXBs offers us much more and that makes them so riveting and fascinating to study. So what makes them so interesting?

- They enable us to constrain the evolution of binary star systems.

- They allow us to set their mass/size constrains and study their fundamental properties.

- We are able to gain insight into exotic end-points of stellar evolution.

- HMXBs are great objects to study accretion discs and accretion processes in general.

- It is possible to probe physical conditions and processes in extreme conditions, such as near the surface of a neutron star or the event horizon of a black hole.

- Some of them can be considered miniature versions of other exotic objects, most notably active galactic nuclei. However, being closer to us makes them easier to study and the research into HMXBs may provide valuable insight into the inner workings of these much more violent and distant objects.

Chapter 2

High Mass X-ray binaries Zoo

Even though X-ray binaries are divided, mainly according to the mass of the secondary star, into two main categories: LMXBs and HMXBs, it would be erroneous to assume that these groups are homogeneous. On the contrary, they comprise different types of objects in different configurations with various physical processes involved, making a complete classification an effortful task as there are some objects that are so unique they could be a distinct class by themselves. This is especially true for HMXBs.

Figure 2.1: An artist's impression of a well-known HMXB Cyg X-1. Image courtesy ESA/Hubble

2.1   Be/X-ray binaries

Based on the luminosity class of the secondary star, HMXBs are further classified into Be/X-ray binaries and supergiant X-ray binaries. The Be/X-ray binaries (Be/XBs) currently represent the largest subclass of HMXBs, which is true especially for those in Magellanic clouds. However, we are quite unsure of their numbers: Meurs & van den Heuvel estimate 2000 – 20000 Be/X-ray Binaries in the Galaxy[11]. Currently, about two thirds of the identified systems fall into this category.

In these systems, the secondary star is either a dwarf, subgiant or a giant OBe star (luminosity class of III, IV or V) which shows spectral lines in emission. Generally, it is a

fast-rotating B-type star that is still on the main sequence and lying well inside the Roche surface which at some point of its life shown spectral lines in emission, hence the qualifier 'e' in its spectral type. The best studied lines are Paschen and Balmer series of hydrogen but these stars may also show He and Fe emission lines. They also show a larger amount of infrared radiation than is expected from an absorbtion-line B star of the same spectral type. This extra emission is known as infrared excess. The origin of the emission lines and infrared excess in Be/X-ray binaries is attributed to an equatorial disk, fed from material expelled from the rapidly rotating Be star in a manner that is not yet understood. The compact object is a neutron star and is typically in a wide, moderately eccentric orbit with an orbital period in the range of 16 – 400 days, and it spends little time in close proximity to the dense circumstellar disk surrounding its companion. No black hole system has been found yet.

Mass transfer from the secondary to the primary takes place during periastron, when the neutron star passes close to this disk, sometimes even passing right through it. X-ray outbursts are expected when the compact object passes throught the disk, accreting from the low-velocity and high-density wind around the secondary (collectively termed Be/X-ray transients). The X-ray spectra of these Be/X-ray binaries are usually hard (There are two spectral states for X-ray binaries: a soft (high) state when a pronounced black body spectrum is visible with a temperature about 1keV and the luminosity is high, and a hard (low) state when the blackbody emission disappears and the X-rays are emitted in the hard X-ray region up to 150 keV. The existence of these two states is generally interpreted as evidence for two distinct modes of accretion. When the accretion rate is high, the soft flux is dominant and this would correspond to a soft state. Conversely, low accretion rate corresponds to a hard state. One can refer to the book by Camenzind[12] for a detailed understanding of this topic.) The hard X-ray spectrum, along with the transience, are important characteristics of the Be/X-ray binaries.

There is an evidence suggesting that there are two distinct subpopulations of Be/X-ray binaries, probably associated with two distinct types of neutron-star-forming supernova, with electron-capture supernovae preferentially producing systems with shorter spin periods, shorter orbital periods, low eccentricities, lower space velocities and somewhat less massive neutron stars, while iron-core-collapse supernovae tend to produce systems with longer spin and orbital periods, high eccentricities, high space velocities and more massive neutron stars. [5],[6],[13],[14],[15].

2.2 Supergiant X-ray binaries

Systems belonging to the second group of HMXBs, known as supergiant X-ray binaries (SGXBs), contain a compact object and a star of luminosity class I or II. In such systems, the compact object orbits the supergiant early-type star, deep inside the highly supersonic wind. The star emits a substantial stellar wind with a mass loss rate of $10^{-6} - 10^{-8} \, \mathrm{M_\odot \, yr^{-1}}$ with a terminal velocity up to 2000 $\mathrm{km \, s^{-1}}$. According to the dominant mode of mass transfer we can subdivide SGXBs into two main subgroups: a) systems fed by the capture of the stellar wind of the secondary companion and b) Roche lobe overflow-fed systems. In some systems, both of these mass transfer mechanisms might be taking place[16].

In spite of the fact that the capture from a high-velocity stellar wind is inefficient,

the large mass-loss rate in the wind can result in an appreciable mass accretion rate onto the neutron star that is sufficient to emit X-ray radiation. The majority of SGXBs are wind-fed, Vela X-1 being the best known member of this group. Wind-fed SGXBs are close systems with an orbital period under 15 days and a low eccentricity. Because of this the X-ray emission is persistent ($L_x \sim 10^{35-36} \, \mathrm{erg\,s^{-1}}$), outbursts may occur as well. Because of wind inhomogenities, these systems may exhibit large variations in brightness on relatively short timescales.

In the case of Roche lobe overflow-fed systems, the secondary star fills its Roche lobe and this results in a transfer of material to the compact object via the first Lagrange point and forms an accretion disk around it. Such process results in a mass transfer rate that is much larger than by the capture of the stellar wind alone. This causes much higher luminosity ($L_x \sim 10^{38} \, \mathrm{erg\,s^{-1}}$) during outbursts. Roche lobe overflow-fed SGXBs are usually persistent sources. Only three sources that belong into this group are known so far: Cen X-3, SMC X-1 and LMC X-4, only one of them being in our Galaxy. The X-ray photons emitted from the compact object by either of the accretion processes, must propagate through the stellar wind to the observer, resulting in absorbtion, scattering and reprocessing of the X-ray emission.

Due to their brightness and persistent X-ray emission, SGXBs were among the first HMXBs to be discovered. They were initially thought to represent the dominant population of HMXBs, whereas Be/X-ray binaries were considered atypical cases. Hence, the name classical or standard was given to SGXBs despite their smaller population.[5],[6],[14],[17]

2.3 Odds and ends — other types of HMXBs

The well established framework of HMXB classification into two classes: SGXBs (further divided into wind-fed or disk-fed) and Be/XBs (either transient or persistent) may not always be sufficient for more compex situations that arise when newly discovered systems may not fit well into either of these categories.

2.3.1 Low eccentricity Be/XBs

This is a group consisting only of five Be/XBs: X Per, 2S 1553-542, GS 0834-430, KS1947+300 and XTE J1543-568, having orbital periods over 30 days. As their name implies, the main discerning characteristic of the group are very low eccentricities of these systems, only $e < 0.2$. This means that the neutron star received an unusually low velocity at birth. However, this seems to be impossible, as most accepted models for neutron star formation predict that neutron stars receive kicks with velocities about 100 - 200 $\mathrm{km\,s^{-1}}$. Thus, such systems should not exist but that is clearly not the case. A plausible explanation seems to be the one given by Pfahl et al.[18]. They propose that a neutron star receives a relatively small kick if the star goes through an electron capture supernova. Since the compact cores associated with electron capture supernovae are smaller, it is much easier to eject the envelope. This is likely to lead to a prompt explosion, where the instabilities causing large kicks do not have enough time to develop [14],[18],[19].

2.3.2 Obscured sources and Supergiant fast X-ray transients

There is a population of highly obscured HMXBs with supergiant companions and a new type of source that displays outbursts that are significantly shorter than typical of Be/XBs and which are characterized by bright flares with a duration of a several hours and peak luminosities of normally $10^{36} - 10^{37} \, \mathrm{erg \, s^{-1}}$. These new systems, unveiled by INTEGRAL, have been named Supergiant fast X-ray transients (SFXTs). Both SFXTs and obscured HMXBs display X-ray and IR spectra that are typical for SGXBs. The current theory behind these systems is that the binary is shrouded in a very dense and absorbing circumstellar material envelope, similar to a cocoon, made of cold gas and/or dust. There are several models attempting to explain the inner workings of SFXTs. The most promising model assumes the presence of clumpy stellar wind. The outburst then occurs as a result of accretion of one of these clumps. Another model assumes a highly eccentric orbit of the system. Outbursts are then triggered as the compact object passes through the periastron. There is also a possibility that compact objects in SFXTs are in fact strongly magnetized neutron stars. These objects remain to be shrouded in enigma and their classification is hazy at best. For a more detailed discussion of these systems one might consult a paper by Chaty(2010)[20].[14]

2.3.3 γ-ray binaries

This is a group of only a handful of exotic systems radiating the most of their output in MeV – TeV range. The secondary star in such systems can be either a luminous O star, a Be star, or possibly a Wolf-Rayet star. All confirmed γ-ray binaries show a jet or jet-like radio structure, which hints the presence of relativistic particles. The dominant physical mechanism to produce the γ-ray radiation and its orbital modulation depend on the specific type of a secondary star present in the system. If the primary is a pulsar and a secondary is very massive and produces a high-density field of ultraviolet photons, the main mechanism would be the up-scattering of UV photons from charged particles up to γ-ray energies. Another scenario is when the secondary is replaced by a star of Be type. Such stars are characterized by a massive outflow with disk and/or flattened envelope geometry, in fast rotation. The γ-rays are then produced by the interaction of the pulsar wind with the ions in the massive outflow. The jets present in these systems are also likely the origin of the very-high energy γ-rays.[14],[21],[22]

2.3.4 γ Cas like objects

The optical properties of this class of systems are similar to Be/XBs, however they differ from them in the X-ray properties. Two models are proposed to explain this type of systems: accretion on the compact object (most likely a white dwarf) and magnetically heated material between the photosphere of the B star and the inner part of its disk.[14]

Chapter 3

HMXBs, bow shocks and hyper velocities

High Mass X-ray binaries, as the name suggests, have been predominantly investigated in the X-ray part of the spectra. However, multispectral studies of these systems may provide the potential for a more complete solution of a HMXB's parameters. That includes not only the observations of the stars themselves, but also some of the secondary attributes of the system as well, most notably stellar bow shocks. Indeed, stellar bow shocks are useful probes of the interstellar medium, the system and the stellar wind velocities. Especially the latter two attributes are particulary useful when studying HMXBs, as these systems are suspected to have large space velocities but often the proper motion and the distance of the system are poorly known. A lot of HMXBs are wind-fed, so the stellar wind velocities that can be inferred from the bow shock might provide a lot of insight into the system, especially when linking to the data obtained in the higher energies.

The physical investigation of the shocks in space is a work in progress and involves lots of advanced physics and mathematics especially in the areas of fluid dynamics, thermodynamics and modelling. In this section we will leave these parts out, instead, we will concentrate more on the relevant equations that may help us determine the parameters of the observed HMXBs.

3.1   A primer on stellar bow shocks

Shock features occur in bullet motions, explosions, as well as in astrophysics. To have a shock wave, we need a motion comparable or exceeding the sound speed. To illustrate how these waves arise, let us consider the one-dimensional flow of gas in a cylindrical tube with a small diameter, which is fit with a piston at one end and closed at the other end. As the piston is moved into the fluid, the fluid starts to compress. Information about this rise in pressure propagates away from the piston at the sound speed c_s of the fluid. If the piston speed v_p is greater than the sound speed, the pressure continues to build in front of the piston with the gradient in pressure becoming steeper and steeper. The edge of the pressure hump (the shock) moves down the tube at the speed v_s. From this, we can define the Mach number as:

$$M = \frac{v_s}{c_s}. \tag{3.1}$$

We can distinguish between isothermal and adiabatic shocks. If there is a very efficient cooling by radiation present, the shock may behave isothermally instead of adiabatically. Such shocks differ from the adiabatic ones in that the speed of sound is lower than in adiabatic shocks and jump conditions are different. In real life situations, we encounter shocks that are a compromise between these two types. However, the shocks in space are better described by the adiabatic shock theory.

If we consider a frame of reference where the bow shock is at rest, we can use a set of equations to obtain the relative conditions before and after the shock, specifically the density, pressure and flux conditions. These equations, callled Rankine-Hugenoit equations, are characterized by the conservation of three quantities: the mass, the flux of momentum and the specific total energy. However, these equations are valid only if the mean free path of the particle is small in comparison with characteristic lengths involved in the problem. In the space, where the medium is so rarified, the conditions for shock seem to be impossible, however, the shock waves do exist as the interstellar medium and stellar wind contain plasma. When dealing with a plasma in a magnetic field, there is a second characteristic length, called the Larmor radius. If this length is much less that the characteristic size of the system, we can transition from hydrodynamics to magnetohydrodynamics (MHD). MHD shocks are similar to adiabatic shocks, but with the addition of a magnetic field term and one more conserved quantity, the magnetic flux. The 'MHD Rankine-Hugenoit equations' have form

$$\rho_1 v_1 = \rho_2 v_2 \tag{3.2}$$

$$p_1 + \rho_1 v_1^2 + \frac{B_1^2}{2\mu_0} = p_2 + \rho_2 v_2^2 + \frac{B_2^2}{2\mu_0} \tag{3.3}$$

$$\frac{1}{2}\rho_1 v_1^3 + \frac{\gamma}{\gamma-1} p_1 \rho_1 + \frac{B_1^2 v_1}{\mu_0} = \frac{1}{2}\rho_2 v_2^3 + \frac{\gamma}{\gamma-1} p_2 \rho_2 + \frac{B_2^2 v_2}{\mu_0} \tag{3.4}$$

$$v_1 B_{\perp 1} = v_2 B_{\perp 2}, \tag{3.5}$$

where ρ, v, p and B are the plasma density, velocity, pressure and magnetic field on respective sides of the shock, γ is the polytropic exponent and μ_0 is the vacuum permeability. Note that by exluding the magnetic terms and omitting the last equation, one can revert to Rankine-Hugenoit equations for adiabatic shocks.[23],[24]
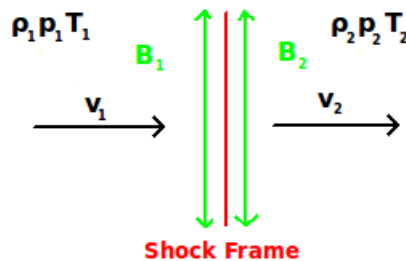

Figure 3.1: Illustration for MHD shock equations, redrawn from the original illustration in [24]

Numerous examples of shocks in space can be found (supernova explosions, Herbig-Haro objects, etc.), but in this work we will concentrate on the stellar bow shocks. Stellar wind bow shocks are structures due to the supersonic passage of wind-blowing stars. They condense the interstellar medium into thin shells, which may be revealed by their post-shock emission or by the scattered light. The symmetry axis of a bow shock generated by a supersonically moving star reflects the direction of motion of the star with respect to the ambient medium, which also could be in motion relative to the local standard of rest at the location of the star. For instance, high-velocity outflows from young star clusters by the collective effect of stellar winds can create bow shocks around low-velocity stars in the cluster halo (LL Ori). When studying the runaway stars located far from star-forming regions and their associated gas outflows, one can assume that the peculiar velocity of the ambient medium is negligible compared to the space velocity of the star, meaning that the symmetry axis of the bow shock coincides well with the direction of the stellar motion. In that case, the orientation of the bow shock can be used to back-trace the trajectory of the star to the parent cluster even for those stars whose proper motions cannot be measured with high confidence.[25]

Figure 3.2: A bow shock-generating runaway star ζ Oph as seen by WISE. Blue and cyan colors represent 3.4 and 4.6 μm light, green represents 12 and red represents 22 μm light. Image courtesy NASA/JPL-Caltech.

The geometry of a bow shock generated by a supersonically moving star is characterized by two main parameters, the Mach number and the stand-off distance R_s. This R_s is the distance from the star where the momentum flux from the stellar wind material of density ρ_w and velocity v_w is equal to the momentum flux from the ambient medium of density ρ_a moving at velocity v_a relative to the star and this is where the bow shock forms. Hence,

$$\frac{1}{2}\rho_w v_w^2 = \frac{1}{2}\rho_a v_a^2. \tag{3.6}$$

The stand-off distance can be expressed as

$$R_s = \left(\frac{\dot{M} v_w}{4\pi \rho_a v_\star} \right)^{\frac{1}{2}},$$ (3.7)

where $\dot{M}$ is the stellar mass-loss rate, v_w and $v_\star$ are the wind and star velocities respectively,

$$\rho_a = 1.4 m_H n,$$ (3.8)

m_H being the mass of a hydrogen atom and n is the number density of the ambient medium. R_s can be measured directly from the bow shock images (provided we know the distance to the object). Technically, only the projected separation, $R_s \cos(i)$, can be measured, but in order to resolve the bow shock morphology, the viewing angle cannot be that far from $i = 0°$, so the $\cos(i)$ is not far from unity.[25], [26]

Bow shocks are also characterized by the Mach number. The higher M (or the $v_\star$), the smaller the opening angle, α, of the bow shock, which is related to the Mach number through the relationship:

$$\alpha = 2 \arcsin(1/M)$$ (3.9)

In practice, however, this angle is difficult to determine owing to the low emission measure of the flanks of bow shocks. Nevertheless, crude estimates may still be made.[25]

3.2 Origin of HMXBs' high velocities

Stars or star systems possessing space velocities exceeding 30 or 40 $km\,s^{-1}$ (this value varies in this range depending on an author) with regard to their local rest-systems are termed runaway stars (or systems), or runaways for short. It has been confirmed by radial velocities and proper motion measurements that a significant portion of HMXBs are runaways. The primary cause for their high velocity is the supernova explosion of one of its components. However, the cluster ejection scenario, where the dynamical interactions in a dense compact cluster may result in the ejection of one or more of its members, is also a viable mechanism of producing runaways (including binaries). In some cases, both of these machanisms might be at work.

HMXBs are the descendants of massive binaries, in which the initially more massive star (the primary) has gone supernova and become a neutron star or a black hole. One would expect that the supernova explosion would disrupt the binary, however, the system remain bound after the supernova due to a phase of mass transfer that occurs in the system when the primary grows larger than its Roche lobe. At that stage of the stellar evolution, the mass transfer does not affect the life expectancy of the primary. As a consequnce, the secondary grows more massive, ultimately becoming more massive than the primary. So when the primary goes supernova, less than half of the total system mass is lost and the system remains bound. So

$$M_{ej} < \frac{1}{2}(M_1 + M_2),$$ (3.10)

where M_1 and M_2 are the pre-supernova masses of the primary and secondary stars, respectively, is a necessary condition to be met. In response to the instant mass loss caused

by the supernova explosion, the binary system recoils with a velocity

$$v = \left(\frac{GM_2}{a_{\text{pre}-\text{SN}}} \right)^{1/2} \left(\frac{M_2}{M_1 + M_2} \right)^{1/2} \frac{M_1 - M_{co}}{M_2 + M_{co}}, \tag{3.11}$$

where G is the gravitational constant, M_{co} is the mass of the compact object (neutron star or a black hole) and $a_{\text{pre}-\text{SN}}$ is the pre-supernova semimajor axis of the binary. From the expression it can be seen that the tightness of the binary before the supernova explosion and $M_{ej} = M_1 - M_{co}$ affect the peculiar velocity the HMXB attains. For most SGXBs the attained velocity should be on the order of 50 km s^{-1} and for a less massive class of Be/XBs it should be about 15 km s^{-1}.

It should be noted that a supernova explosion discussed here is symmetric. In a case of an asymetrical supernova explosion, the additional kick exerted on a compact object upon creation can cause a disruption of the system, or, if the direction of the kick if favorable, the system may attain a speed that is slightly higher than the speed which would result from a symmetric supernova explosion. [25], [28], [27]

3.3   HMXB bow shock surveys

With the advent of modern space based infrared telescopes, many surveys searching for bow shock features around runaway stars have been conducted. One of the notable examples is E-BOSS: An Extensive stellar BOw Shock Survey[29], mostly focused on OB stars. Despite this, HMXBs have received little atention so far.

Bow shocks associated with HMXBs are thought to be extremely rare as they have a high probability to be enclosed in the hot and rarefied regions (superbubles) that surround OB associations, where the speed of sound is higher than the speed of most runaways.[30]. Finding one is thus a discovery of significant scientific importance.

The first bow shock survey of HMXBs was conducted by Huthoff & Kaper (2002)[30]. They chose a sample of 11 HMXBs for which the conditions for a bow shock formation seemed favorable: a large space velocity and an OB companion with a strong stellar wind and a high luminosity. Their survey utilized high-resolution IRAS maps and they detected only an infrared counterpart to the already known bow shock generated by Vela X-1.

Another survey was conducted by Gvaramadze et al. (2011)[25] on the same sample that Huthoff & Kaper (2002) used. They utilized the data from the Spitzer Space Telescope, which were of higher quality but they covered only 5 of 11 HMXB from the original sample. Nevertheless, they were able to discover a new bow shock around 4U 1907+09 and detected Vela X-1 bow shock as well.

As there are more than a hundred suspected and confirmed HMXBs and the wealth of archival data available we saw an opportunity to expand this search, including all suspected and confirmed HMXBs known up to date using the data from the Spitzer Space Telescope and Wide-field Infrared Survey Explorer (WISE). Combining superior resolution of the Spitzer image data with an almost 100 % sky coverage of the WISE data we were able to obtain an unprecedented view of HMXBs in these bands, allowing a complete bow shock survey to be conducted.

3.4   Peculiar velocity determination cookbook

Modern astrometric missions such as Hipparcos and astrometric surveys conducted in this or the previous century enable us to determine the proper motions of a lot of stars with a considerable accuracy. This is absolutely crucial for studying runaway systems possessing high peculiar velocities. If the distance to the system is known, the proper motion data can be used to determine the tangential velocity of the system and, from this, even its peculiar tangential velocity. Here we calculate the peculiar velocities via the method used by Mdzinarishvili & Chargeishvili (2005)[31].

If we assume that we have the proper motion data in equatorial coordinates available, the first step is to calculate the proper motion components μ_l and μ_b in the Galactic coordinate system:

$$\mu_l = \mu_\alpha \cos \psi + \mu_\delta \sin \psi, \tag{3.12}$$

$$\mu_b = -\mu_\alpha \sin \psi + \mu_\delta \cos \psi, \tag{3.13}$$

where ψ – the parallactic angle is obtained from:

$$\cos \psi = \frac{\sin \delta_G \cos \delta - \cos \delta_G \sin \delta \cos(\alpha - \alpha_G)}{\cos b}, \tag{3.14}$$

$$\sin \psi = \frac{\sin(\alpha - \alpha_G) \cos \delta_G}{\cos b}, \tag{3.15}$$

where α, δ are the equatorial coordinates of a star,

$$\mu_\alpha = \frac{d\alpha}{dt} \cos \delta, \ \mu_\delta = \frac{d\delta}{dt} \tag{3.16}$$

are components of proper motion in the equatorial coordinate system,

$$\mu_l = \frac{dl}{dt} \cos b, \ \mu_b = \frac{db}{dt} \tag{3.17}$$

are components of proper motion in the Galactic coordinate system (l, b). $\alpha_G = 192.85948°$ and $\delta_G = 27.12825°$ are the coordinates of the Galactic pole (epoch 1991.25). Now, we can calculate the observed tangential velocity (in $km\,s^{-1}$) components via the well-known equations:

$$v_{lt} = 4.74r\mu_l, \tag{3.18}$$

$$v_{bt} = 4.74r\mu_b, \tag{3.19}$$

where r is the distance to the system in kpc and μ_l, μ_b are given in milliarcseconds/year (mas/yr). To obtain the peculiar tangential velocity of the system it should be noted that:

$$v_{lt} = (v_{lt})_\odot + (v_{lt})_{rot} + (v_{lt})_{pec}, \tag{3.20}$$

$$v_{bt} = (v_{bt})_\odot + (v_{bt})_{rot} + (v_{bt})_{pec}. \tag{3.21}$$

$(v_{lt})_\odot$ and $(v_{bt})_\odot$ represent the solar peculiar motion:

$$(v_{lt})_\odot = U_\odot \sin l - V_\odot \cos l, \tag{3.22}$$

$$(v_{bt})_{\odot} = U_{\odot} \cos l \sin b + V_{\odot} \sin l \sin b - W_{\odot} \cos b, \tag{3.23}$$

$(U_{\odot}, V_{\odot}, W_{\odot}) = (10.0, 11.0, 7.2) \mathrm{km\,s^{-1}}$ are adopted in this work but they may vary a bit depending on the author. Galactic rotation is expressed as:

$$(v_{lt})_{rot} = R_0(\omega - \omega_0) \cos l - \omega r \cos b, \tag{3.24}$$

$$(v_{bt})_{rot} = -R_0(\omega - \omega_0) \sin b \cos l, \tag{3.25}$$

ω and ω_0 can be determined via:

$$R^2 = R_0^2 + r^2 \cos^2 b - 2rR_0 \cos b \cos l. \tag{3.26}$$

If we assume a flat rotation ($V_0 = \mathrm{const}$) for galactocentric distances (in kpc) $3 \leq R \leq 18$, we can adopt $\omega = \frac{V_0}{R}$ and $\omega_0 = \frac{V_0}{R_0}$, where $R_0 = 8$ kpc is the solar galactocentric distance and $V_0 = 240 \mathrm{km\,s^{-1}}$ is the circular Galactic rotational velocity.[31] If we are dealing with the objects that are outside this distance range, we need to adopt a new value of V for the object from Clemens (1985)[32].

Finally, after calculating the peculiar tangential velocity components of the system, for the total peculiar tangential velocity we have:

$$(v_t)_{pec} = \sqrt{(v_{lt})_{pec}^2 + (v_{bt})_{pec}^2}. \tag{3.27}$$

In this work, we assume the errors in peculiar velocities are only due to the uncertainities in the proper motion determination.

Chapter 4

Data Acquisition and reduction

4.1   Spitzer Space Telescope

The Spitzer Space Telescope (formerly known as the Space Infrared Telescope Facility) is the last of the NASA Great Observatories program, covering the spectral regions from mid to far infrared. Launched in 2003, it was expected to operate for 2.5 years with the possibility of prolonged operation after the depletion of the liquid helium coolant supply. As the infrared instruments onboard need to be cooled to very low temperatures to function, after the coolant exhaustion in May 2009 most of them became no longer usable. However, after May 2009, Spitzer Space Telescope continues to operate with limited capabilities as the Spitzer Warm Mission. Spitzer carries three instruments onboard: IRAC (Infrared Array Camera)[33], IRS (Infrared Spectrograph)[34] and MIPS (Multiband Imaging Photometer for Spitzer)[35]. [36]
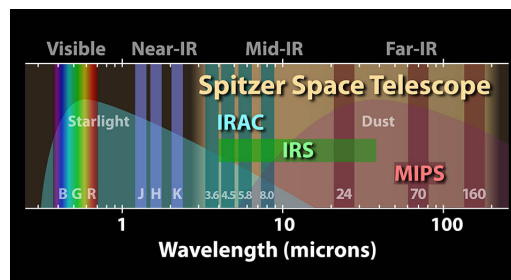
Figure 4.1: The Spitzer Space Telescope spectral coverage. Image courtesy NASA/JPL-Caltech.

4.1.1   MIPS

The Multiband Imaging Photometer for Spitzer (MIPS) provides the Spitzer Space Telescope with capabilities for imaging and photometry in broad spectral bands centered nominally at 24, 70, and 160 μm, and for low-resolution spectroscopy between 55 and 95 μm. The instrument contains 3 separate detector arrays (128x128 pixel Si:As, 32x32 pixel Ge:Ga, 2x20 stressed Ge:Ga), providing high-sensitivity, low-noise, diffraction-limited performance. In this work, we use the data only from the short-wavelength 24 μm detector

Figure 4.2: An artist's impression of The Spitzer Space Telescope. Image courtesy NASA/JPL-Caltech.

giving a bandpass from 20.8 to 26.1 μm with a weighted average wavelength of 23.68 μm, having approximately 5′ field of view (FOV) and the point spread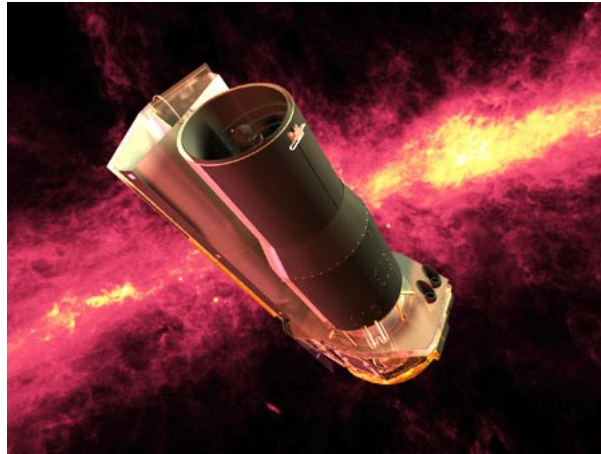 function (PSF) size of 6″ full width at half maximum. For more information one may refer to MIPS Instrument Handbook[37].

The MIPS data for a particular object may be obtained by querying the Spitzer Heritage Archive. The archive will list the relevant Astronomical Observation Requests (AORs), which are fundamental units of Spitzer observing which can be packed into a .zip file and downloaded. An AOR normally contains the calibration data, Data Collection Events (DCEs) which are single frame exposures (also refered to as 'raw' or Level 0 Data), Basic Calibrated Data (BCDs) and Post-BCDs (PBCDs). BCDs, also known as Level 1 Data, are the data products derived from DCEs, having been run through the Spitzer online calibration pipeline and have had some basic artifact clean-ups applied (orentation flipping, dark substraction, flat field correction, conversion into units of MJy/sr). They are designed to be the most reliable product achievable by automated processing. Post-BCDs, or Level 2 Data, are the data products derived from a full AOR, e.g., a combination of several BCDs. Post-BCD products most commonly include mosaics. MIPS BCDs and PBCDs products are 2-dimensional FITS images with a full set of header keywords, calibrated in MegaJanskys per steradian (MJy/sr).

Normally, the PBCD pipelines handle 24 μm data relatively well, enabling immediate detailed analysis, however, in our case, the quality of PBCD products was completely unsuitable to our needs. Despite that, using PBCDs we were able to ascertain whether the AOR contains the object or not (a PBCD is a product of all BCDs in an AOR), as the search query often lists AORs that do not contain the searched object at all. By checking PBCDs, we were able to sort through all AORs in the search query and run the pipeline only for the relevant ones. Doing so, we were able to save several hours (varies with the computing power) of computing time for each pipeline that would be run futilely. With a large number of objects surveyed, this translates into several days of saved computing time. However, for the image analysis, we needed to revert to using the BCD products, create a custom pipeline and make our own PBCD products.
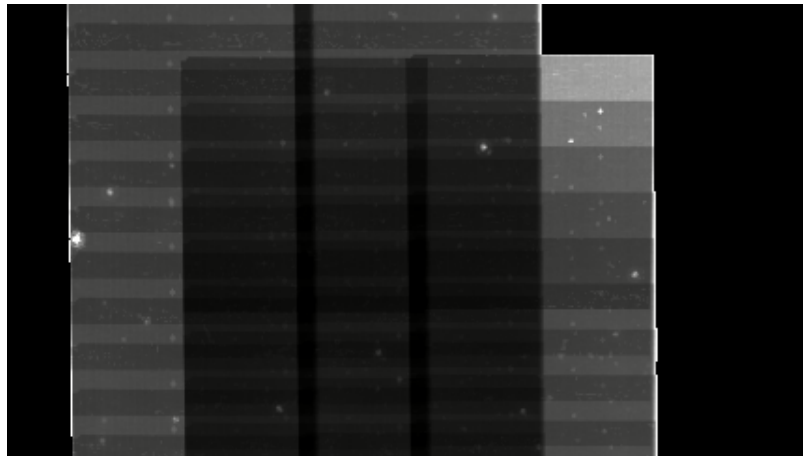
Figure 4.3: An an example of a cut-out from a patchy PBCD mosaic obtained from an AOR containing 4U 1907+09 (a HMXB). Note that the stars are noticable but the seams between the component images make it difficult to discern any fine structures in the image.

The BCD data normally consist of *bcd.fits (the image data), *bunc.fits (the uncertainity images that correspond to the image data) and *bbmsk.fits (the mask images that flag temporarily bad pixels in the input data files) files. We will use these data files to create our own products via MOPEX (MOsaicking and Point source EXtraction, which is a package developed at the Spitzer Science Center for astronomical image processing). MOPEX can be run on the command line or with a graphical user interface and has several major components that can operate together as one pipeline or separately on different sets of data. The major components are 'Overlap', 'Mosaic', 'APEX multi-frame' and 'APEX single frame'. Overlap is designed to remove image background variations due to foreground light sources. Mosaic removes defects and spurious pixels (e.g. cosmic rays), reassembles the data onto a common pixel grid, and combines your data into a science grade mosaic with a corresponding noise map. The two APEX modules find objects and measure photometry on the final calibrated data and are not used in this work. The GUI is laid out as a data flow diagram. The first box specifies the input data and each subsequent box represents a module in the data reduction pipeline. Each module acts on the data from previous module and the passes the data to the next module in the order specified by the GUI window.

The first step in the processing is the creation of the file lists that will be fed to the pipeline. When working in a UNIX-based system, this task can be easily done by using the ls command.

```
unix% ls /<data_dir>/ch1/bcd/*bcd.fits > bcdlist.txt
unix% ls /<data_dir>/ch1/bcd/*bunc.fits > bunclist.txt
unix% ls /<data_dir>/ch1/bcd/*bbmsk.fits > bbmsklist.txt
```

Next, it is a good idea to remove the first file from each created list. The first frame of each AOR is problematic (shorter exposure time, depressed response) and should be removed from the list of BCDs. This is known as the 'first frame effect'. These always have the number 0000_*0000 in their name so we removed those frame from our file lists. As the AORs we worked with have a good coverage, excluding these frames did not create any adverse effects.
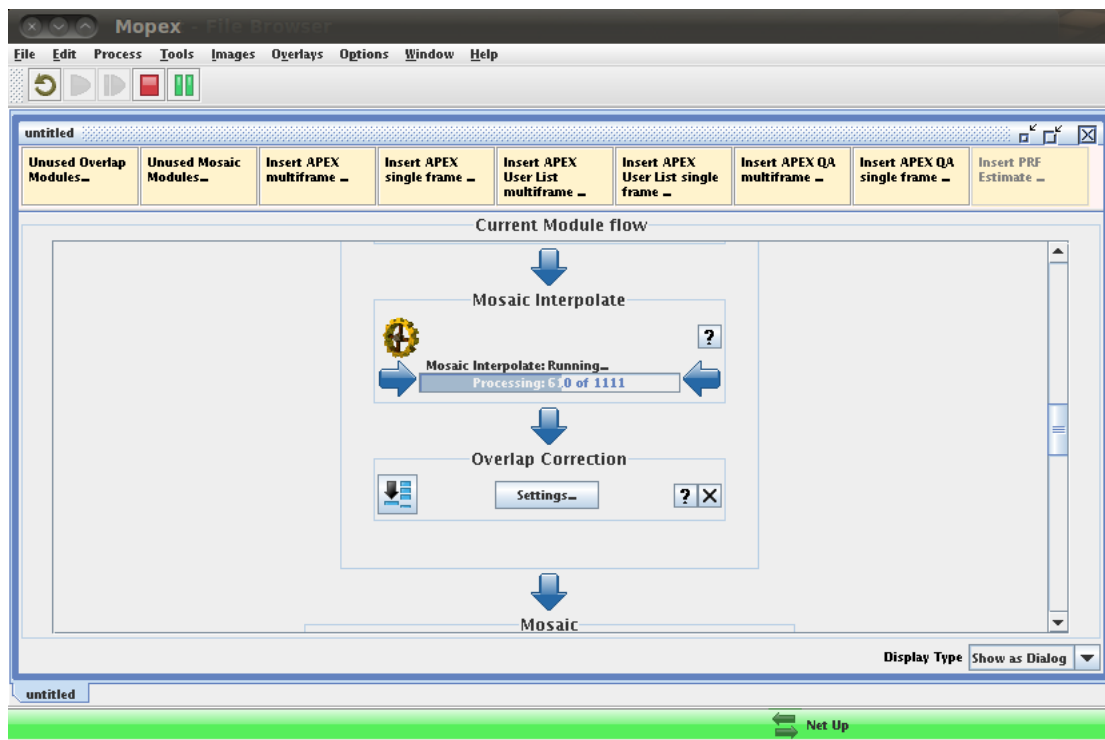
Figure 4.4: The MOPEX GUI with Mosaic Interpolate module running

The first step in processing the MIPS data is the Overlap pipeline. It corrects for variable background levels in your data by finding the additive offsets to each frame so that the pixel differences (after the interpolation to a common grid) are minimized. This requires generating a first pass mosiac and masking objects which may contribute to the background. The default settings that are loaded from the templates in MOPEX are optimal for the most cases. However, if you have very extended objects, a crowded field, or extended emission in your field you may want to adjust some parameters. For the pipeline to run, we need to load our previously created list containing the image, uncertainity and mask files and specify the output directory where the products will be stored. It is also a good idea to include the bad pixel mask (pmask, permanently damaged pixel mask), that is provided with the MOPEX installation or can be downloaded from the Spitzer website. After specifing these files, the Overlap pipeline can be run. The main processing stages of the Overlap pipeline are bright objects masking, interpolation and background matching and involve several modules:

- Fiducial Image Frame: creates a table specifying a unified coordinate system and the spatial boundaries of the output mosaic.

- Med Filter and Detect: the bright objects masking step. These two modules mask bright objects that can bias the background levels of the images in which they are present.

- Mosaic Interpolate: the interpolation step. The input images are interpolated onto the output grid defined by the Fiducial Image Frame (FIF) table.

- Overlap Correction: the background matching step. This module calculates an offset to apply to each image in order to set their backgrounds to a constant value.

Naturally, each module depends on the previous ones, so they must be run in this order for the pipeline to work.

To produce a science grade mosaic we run the Mosaic pipeline. Similarly to the Overlap pipeline, the Mosaic pipeline involves several steps carried out by the Mosaic modules:

- Fiducial Image Frame: as in the Overlap pipeline.

- Mosaic Interpolate and Mosaic Coverage: the input images are interpolated onto the output grid defined by the FIF table.

- Mosaic Outlier: detects radiation hits, bad pixels and moving objects.

- Mosaic R Mask: combines the outlier information into a single mask.

- Mosaic Reinterpolate: updates the interpolated images to iclude the outlier rejection information obtained in the previous steps.

- Mosaic CoAdder and Mosaic Combiner: the interpolated images, uncertainty images and coverage maps are co-added to create respective mosaic images. The default method is computing the straight average of the input pixel values but other options are available as well.

A reduction following these steps will produce a single mosaicked image of all input images, a coverage mosaic showing how many frames were combined to produce each pixel in the output mosaic and an uncertainity mosaic showing the uncertainities at each point of the mosaic.

The following steps were part of the standard processing applied to all datasets. If a bow shock or any peculiar structure was detected in the image we processed the data again, making minor changes to the pipelines according to the presence of extended emission, crowded field and coverage of the dataset. Namely, we changed the outlier detection methods. One of these methods, Mosaic Outlier uses multiple frames to reject bad pixels. It measures the median and sigma for each pixel in the final mosaic and flags stray pixels. This method works best when you have coverage greater than 10 frames per pixel so that the sigma and median are well determined. This was a method of choice when dealing with the AORs dedicated to a certain object as they have a very high coverage. However, the AORs used for various survey data or a large area imaging normally have the coverage less than 10. In this case we added Mosaic Box Outlier, which performs outlier rejection using a method similar to Mosaic Outlier module, but considers a window around each pixel rather than just a single pixel. This is used for moderate coverage where Mosaic Outlier module may miss some real outliers. We also altered the method of intepolation. We used 'drizzle' interpolation method instead of 'default' if the coverage was 10 or more, as this improves the image quality by a small amount (the differents tradeoffs when choosing the method of interpolation are a bit complicated and can be found in MOPEX User's Guide).

As the data reduction involves a lot of fine-tuning and changing the parameters of modules one can save the processing flow as a namelist file which can be then loaded

again in either the command line version of MOPEX or the GUI so one do not have to painstakingly specify the pipeline parameters again. Thus, we created a few namelists which we then simply loaded and executed if we detected any peculiar object, saving us some time and effort. For a more extensive and elaborate explanation of the pipelines and MIPS data reduction one may consult Spizter Data Processing Cookbook[38], MIPS Instrument Handbook[37] and MOPEX User's Guide[39].

4.1.2 IRAC

Infrared Array Camera (IRAC) provides $5.22'$x$5.22'$ images at 3.6, 4.5, 5.8 and 8 μm. All four detector arrays in the camera are 256x256 pixels in size, with a pixel size approximately $1.2''$x$1.2''$. The first two short wavelength channels use In:Sb detector arrays while the other two channels use Si:As detectors. In this work, we used the IRAC data from all its channels when conducting the follow-up observations, as we did not expect significantly strong bow shock emission in these bands. More information on IRAC can be found in IRAC Instrument Handbook[40].

The way in which the data from IRAC is retrieved and handled is very similar to the MIPS data. Similarly, the PBCD and BCD products contained in an AOR are retrieved from the Spitzer Heritage Archive and, yet again, the PBCDs exhibit the same 'patchiness' so a custom reduction became necessary. The BCD data include *bcd.fits, *bunc.fits and *bimsk.fits (equivalent of bbmsk in MIPS) files. The processing was carried out via MOPEX pipelines Overlap and Mosaic. The processing steps involved and the logic behind them are very similar to the ones taken when working with the MIPS data. The pipelines that have been tailored to handle the data from the each channel of IRAC (can be loaded in MOPEX) usually perform spectacularly well but, as above, one may achieve better results by tweaking the pipeline parameters (changing the methods of interpolation, outlier detection etc.) according to the data coverage and the characteristics of the field being imaged.

4.1.3 IRS

The Infrared Spectrograph (IRS) provided spectroscopic capabilities of Spitzer Space Telescope, however, it is now unoperational after the coolant depletion. It consisted of four separate modules (refered to in Spitzer documentation as Short-Low, Short-High, Long-Low and Long-High) and provided low (R$\sim$ 60–130) and moderate (R$\sim$ 600) resolution spectroscopic capabilities from 5.2 to 38 μm. The low-resolution modules employed long-slit designs that allowed both spectral and one-dimensional spatial information to be acquired simultaneously on the same detector array. The high-resolution modules used a cross-dispersed echelle design that allowed broad spectral coverage in a single exposure. In addition, the IRS provided imaging in two filters (13–18 and 18–26 μm) and onboard software to autonomously identify point sources and accurately place them (by offsetting the telescope) in any of the IRS slits. These peak-up arrays were also used to obtain calibrated images of the sky at 16 and 22 μm over a 1x1 square arcminute field of view, providing the only imaging capability of Spitzer between 8 and 24 μm. In this work, we only used the data from the Short-High and Long-High modules, so the description of the

other modules and peak-up arrays will be omitted (details on these topics can be found in IRS Instrument Handbook[41]).

The Short-High (SH) module is a cross-dispersed echelle spectrograph that covers, with a single pointing, the nominal spectral range from 9.9–19.6 μm at R$\sim$ 600. It has a small wavelength overlap (18.7–19.6 μm) with the Long-High module. The detector is a 128x128 pixel Si:As BIB array with a plate scale of 2.3 arcsec/pixel. The SH aperture is a single slit of size 2x5 pixels. The Long-High module is a cross-dispersed echelle spectrograph which covers, with a single pointing, the nominal spectral range from 18.7–37.2 μm at R$\sim$ 600. The detector is a 128x128 pixel Si:As BIB array with a plate scale of 4.5 arcsec/pixel. As with the SH module, the LH aperture is a single slit.

The IRS data may be obtained by querying the Spitzer Heritage Archive. The AORs contain PBCD and BCD directories. The most common BCD products include *bcd.fits (in our case a 2-D echellograms), *bmask.fits (the pixel status masks) and *func.fits (the uncertainity images) files. The PBCD products normally include coadded BCDs and spectral tables (which were not present in our case). Prior to any spectral extraction, it is necessary to visualize our data. It is a good idea to overlay the position of the slits onto an image of the relevant region (the mosaics obtained from IRAC and MIPS data may be the most suitable) via Leopard (a software package used to visualize and download data). In our case, we had a stand-alone AOR for the background substraction, so we had to check for the presence of any objects in the slits that may skew our background estimates.
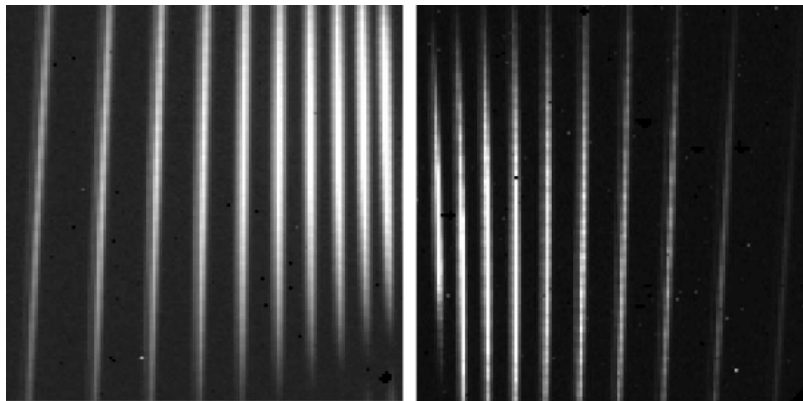

Figure 4.5: A sample of unprocessed data from the Short-High (left) and Long-High (right) modules. Both images show the typical layout of a cross-dispersed echellogram.

The spectra can be obtained via The Spitzer IRS Custom Extraction (SPICE), which provides a JAVA-based tool that allows the user to interactively extract IRS spectra. SPICE can be run on the command line or with a graphical user interface and, as MOPEX, the GUI is laid out as a data flow diagram. To begin using SPICE an extraction flow must be loaded. SPICE flows are initiated using standard templates (point source, extended source, etc.) which are part of SPICE. After overlaying the slit positions on a MIPS mosaic we found out that the studied object fills in the slit so we decided to use 'Extended Source with Regular Extract' extraction flow. In the first step, we must load the echellogram, the pixel status mask and the uncertainty image and specify the directory where the extraction flow products will be saved. SPICE will then automatically fill in the appropriate calibration files that are part of the SPICE distribution. The extraction flow consists of four modules:
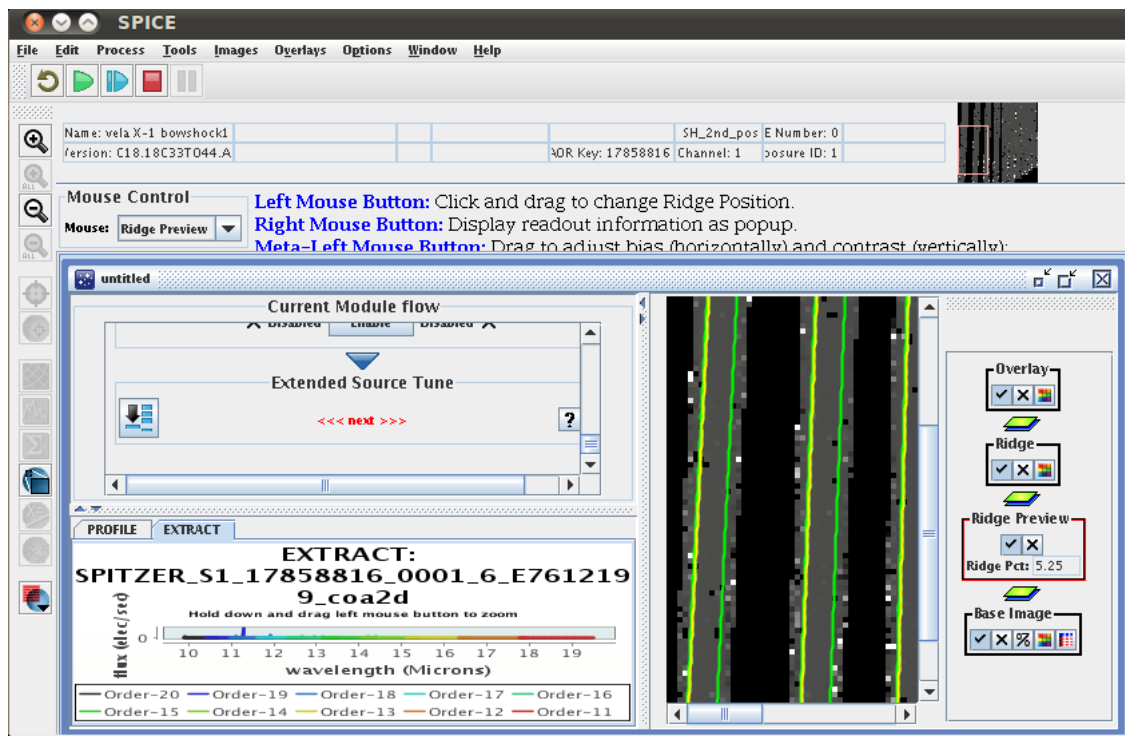
Figure 4.6: SPICE extraction flow.

- Profile: computes and plots the mean spatial flux profile across all user-selected orders.

- Ridge: uses the output from Profile to find the peak in the spatial profile and defines the spectral trace of the source to be extracted.

- Extract: performs spectral extraction within a user-specified window. The resulting spectrum is in units of electron per second.

- Extended Source Tune: converts electrons per second to flux density in Janskys (Jy) and applies the extended source correction.

More details can be found in SPICE User's Guide[42].

Even the processed spectra are not free from artifacts. There are several tools available to mitigate these imperfections, however, they are all IDL-based so we were not able to make use of them. We tried to flag the rogue pixels manually (and most of the should be removed by the background substraction) and the spectra do not seem to suffer from scalloping (order mismatch due to a time-dependent dark-current, scalloped orders would have a shape of the letter 'u'). Despite that, we believe that our spectra may suffer from some residual fringing (brighter and darker dips caused by the interference of light waves in the spectrograph system, common in Short-High and Long-High modules). This imposes certain limits to resolution for a small detail analysis.[42],[41]

4.2   Wide-field Infrared Survey Explorer (WISE)

Operational from December 2009 to February 2011, Wide-field Infrared Survey Explorer (WISE) was NASA's infrared mission. Its main purpose was to perform an all-sky infrared survey in bands centered at 3.4, 4.6, 12 and 22 μm with angular resolution 6.1, 6.4, 6.5 and 12$''$ at each of the channels respectively. WISE utilizes HgCdTe and Si:As detector arrays with a plate scale of 2.75$''$/pixel. Despite the fact that the quality of the data from WISE is lower than the quality of the Spitzer's IRAC and MIPS data, WISE offers far better data coverage of the surveyed objects.
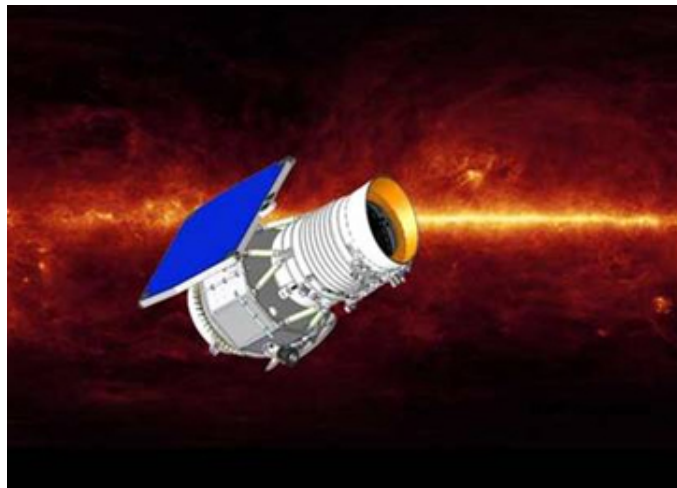
Figure 4.7: An artist's impression of WISE. Image courtesy NASA/JPL.

WISE science data processing, archiving and distribution is performed by the Infrared Processing and Analysis Center (IPAC), California Institute of Technology. The processing software and operations system is based on algorithms, pipelines and architecture used for the 2MASS, Spitzer Space Telescope and GALEX projects. The data seemed to be of sufficient quality for our goals so we queried the WISE Archive for the pipeline-processed (level 3) fits data for the surveyed objects.[43]

It should be noted that the WISE image data have pixel units in DN. When combining this data with the Spitzer image data, one needs to convert DN into MJy/sr. The conversion can be done trivially via IRAF, the parameters can be found in [44].

Chapter 5

Detected bow shocks

5.1 The bow shock survey

We have undertaken a search for bow shocks around the galactic HMXBs from the 4th edition of Catalogue of High Mass X-ray binaries in the Galaxy[5], containing 118 sources in total. Utilizing the archival Wide-field Infrared Survey Explorer (WISE) and Spitzer Space Telescope data, we checked the data available for all the sources in the catalogue. The available data (either Spitzer data, WISE data, or both) covered 102 sources and four bow shocks were detected in total. Two of them, the bow shock associated with Vela X-1 (detected by Huthoff & Kaper (2002)[30]) and the one associated 4U 1907+09 (discovered by Gvaramadze et al. (2011)[25]), are already known. The other two, the ones around the HMXBs 4U 1258-61 and EXO 1722-363, are detected for the first time. The properties of the detected bow shocks and the systems associated with them are discussed below.

Objects surveyed	118
Objects covered by the WISE data	96
Objects covered by the Spitzer-MIPS data	53
Objects covered by the both instruments	47
Objects not covered by either instrument	16

Table 5.1: The coverage of the objects in the original survey contained in Catalogue of high-mass X-ray binaries in the Galaxy, 4th edition.

We decided to conduct the survey in mid-infrared spectral range, via the first channel of MIPS 24 μm and the two long-wavelength channels of WISE: 12 and 22 μm, since the already known bow shocks around HMXBs (and stellar bow shocks in general) show significant emission in this spectral range, not always being visible in near-infrared or the shorter end of mid-infrared. If a bow shock was visible (via the visual inspection of images), we also tried to obtain the data from the other bands.

The all sky data for WISE was released on 14 March 2012, so we were able to expand the survey as the data for the objects not covered by WISE previously had become available. Now, all of 118 known HMXBs and HMXB candidates are covered by, at least, the WISE data. Once again, we looked for bow shocks around these additional 22 HMXBs (or candidates). However, we did not detect any new bow shocks around these objects.

Objects surveyed	118
Objects covered by the WISE data	118
Objects covered by the Spitzer-MIPS data	53
Objects covered by the both instruments	53

Table 5.2: The coverage of the objects in the expanded survey contained in Catalogue of high-mass X-ray binaries in the Galaxy, 4th edition.

The survey is by no means complete, the new systems are discovered and/or re-classified all the time and many systems in the catalogue and thus in the survey are not even confirmed HMXBs. It should be noted that only about a half of the systems are covered by the MIPS data, the other half is only covered by WISE, so it is possible that some other bow shock candidates may have escaped detection.

5.2 Known bow shocks

5.2.1 Vela X-1

Vela X-1 can be considered as one of the most well-known and studied HMXBs. It is a SGXB consisting of super giant HD 77581 and a massive (1.9 M$_\odot$) neutron star in a 8.964 day orbit.[45]

Name	Vela X-1
RA(J2000) [hhmmss,s]	09 02 06.9
Dec(J2000) [° ′ ″]	-40 33 17
Optical counterpart	GP Vel
Opt. Ctp. Spectral type	B0.5 Ib
J; H; K [mag]	5.833; 5.705; 5.596
distance [kpc]	1.9

Table 5.3: Vela X-1 general data.[5]

The bow shock around Vela X-1 was discovered by Kaper et al. (1997)[46] in a Hα image obtained with the 1.54 m Danish telescope at the European Southern Observatory. The original image showed a faint arcuate structure $0.9'$ north of the HMXB system. Since then, it has been observed by Huthoff & Kaper (2002)[30] in IRAS wavelengths and by Gvaramadze et al. (2011)[25] with Spitzer.

The bow shock was detected in all IRAC bands, i.e. at 3.6, 4.5, 5.8 and 8 μm and in 24 μm (MIPS ch.1) as well. Furthermore, Vela X-1 is covered in the newly released all sky data for WISE. The bow shock is visible in all of its channels, i.e. at 3.4, 4.6, 12 and 22 μm.

It has a clear, symmetrical arcuate shape with fine filamentary structures, which are visible in Figure 5.1 and Figure 5.2 as well. There are several cirrus-like structures even beyond the main body of the bow shock, most prominent in the IRAC 8 μm channel. The apex of the bow shock is located $\sim 1'$ from Vela X-1, which at the distance to the system of 1.9 kpc corresponds to the linear separation $R_S \simeq 0.5$ pc.
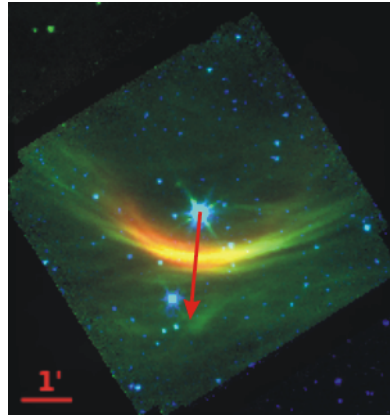
Figure 5.1: A colour image of the bow shock associated with Vela X-1 made from MIPS and IRAC data. Blue shows infrared light with wavelength of 3.6 μm (IRAC ch. 1), green 8.0 μm light (IRAC ch. 4) and red 24 μm light (MIPS ch. 1). The arrow indicates the direction of the computed peculiar motion.
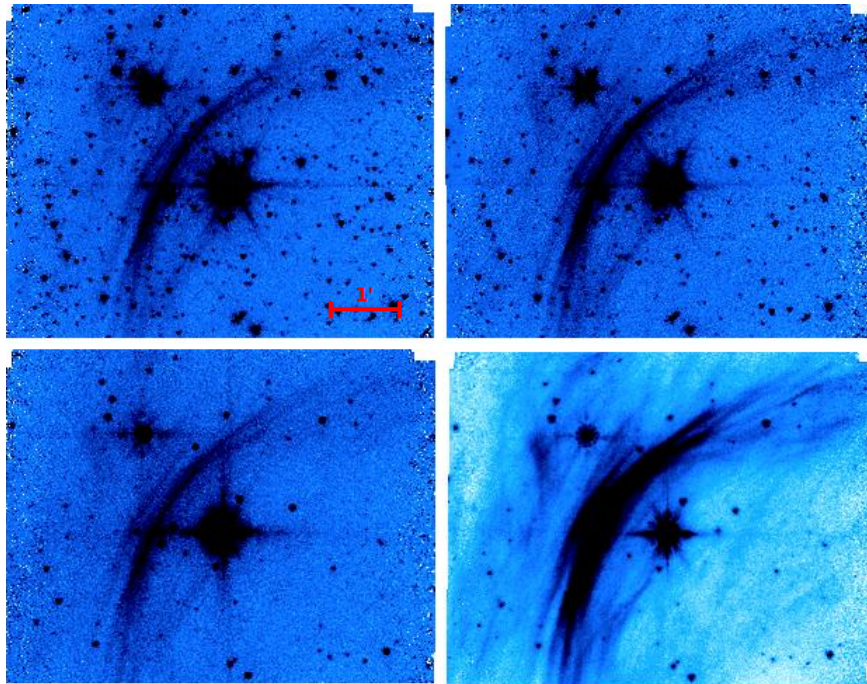
Figure 5.2: IRAC mosaics of Vela X-1 bow shock. From left to right, and from top to bottom: IRAC 3.6, 4.5, 5.8 and 8 μm. There are several wavelength-dependent structures apparent.

We also include the WISE image data of Vela X-1. The decrease in resolution is apparent, but the WISE 12 μm image still shows some fine structures especially on the flanks of the bow shock. It should be noted that this channel is particularly useful in this case, bridging the gap between the last IRAC 8 μm channel and MIPS 24 μm channel.
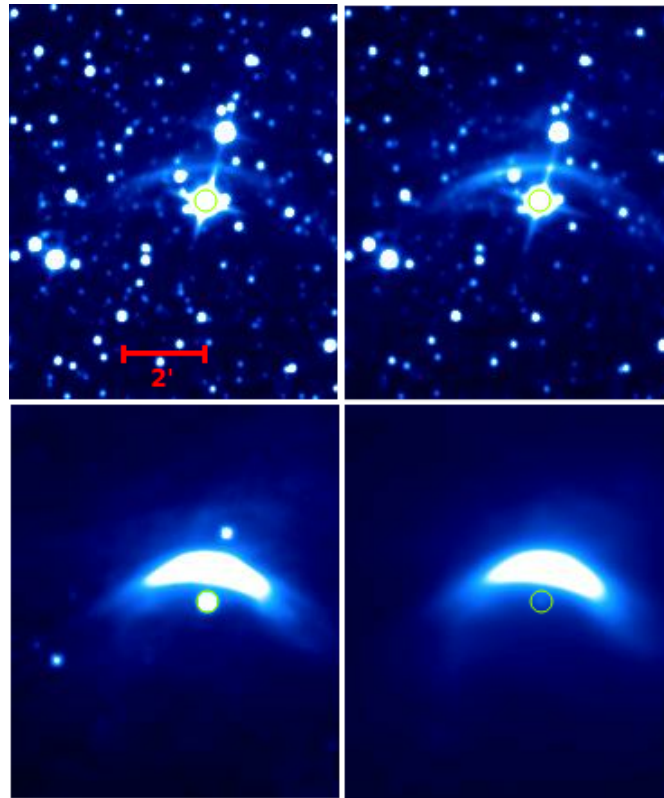
Figure 5.3: WISE images of Vela X-1 bow shock. From left to right, and from top to bottom: WISE 3.4, 4.6, 12 and 22 μm. Note that the system itself is almost invisible on 22 μm, its position is marked by a circle.

5.2.2   4U 1907+09

4U 1907+09 is a system similar to Vela X-1 in many aspects. It is a SGXB housing a neutron star (which is in fact an X-ray pulsar) and a late O-type supergiant star.[25]

Name	4U 1907+09
RA(J2000) [hhmmss,s]	19 09 39.3
Dec(J2000) [° ′ ″]	+09 49 45
Optical counterpart	2MASS J19093804+0949473
Opt. Ctp. Spectral type	O8-9 Ia
J; H; K [mag]	10.00; -; 8.77
distance [kpc]	∼4

Table 5.4: 4U 1907+09 general data.[5],[25]

The bow shock was discovered by Gvaramadze et al. (2011)[25] in the Spitzer data, detecting it at 24 μm. We too have detected the bow shock in this channel, and furthermore, we have detected the bow shock in WISE 22 μm channel as well. WISE 12 μm channel images show a gleam of emission that might be associated with the bow shock, however, any WISE or IRAC channels operating at the shorter wavelengths were not able to pick the bow shock up. Thus, we must conclude that the spectral energy distribution of the bow

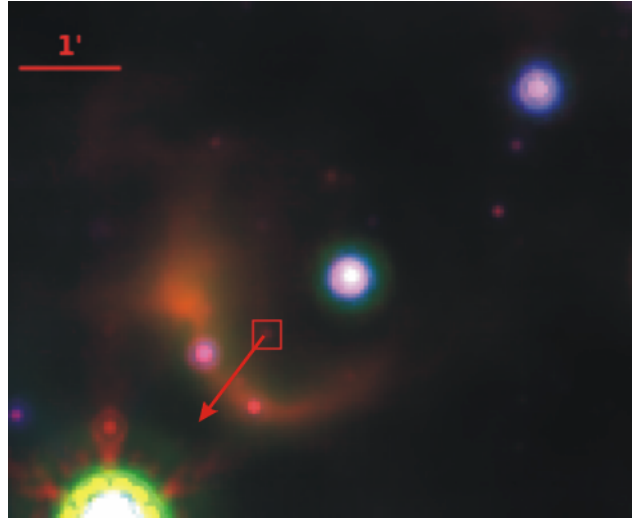shock associated with 4U 1907+09 must be considerably different from that of the one associated with Vela X-1.

Figure 5.4: A colour image of the bow shock associated with 4U 1907+09 made from MIPS and WISE data. Blue shows infrared light with wavelength of 12 μm (WISE ch. 3), green 22 μm light (WISE ch. 4) and red 24 μm light (MIPS ch. 1). The HMXB is marked by the square. The arrow indicates the direction of the computed peculiar motion.

The bow shock itself shows an arcuate shape with three distinct clumps, two of them that are closer to the apex of the bow shock are in fact associated with the emission of the two background/foreground stars, as revealed by the WISE images, and are not features of the shock itself. However, the third clump seems to be a genuine feature. Despite the presence of a background/foreground star at that location, the feature is far too large to be attributed to the emission of the star itself. The apex of the bow shock is about $\sim 0.7'$ from 4U 1907+09 system. At the distance of approximately 4 kpc it would correspond to a linear separation of $R_S \simeq 0.8$ pc.

5.3 New bow shock candidates

5.3.1 4U 1258-61

This system is a Be/X-ray binary, consisting of an X-ray pulsar and and a Be star with a massive equatorially expanding shell of ejected mass.[47]

Unfortunately, this system is not covered by any of the Spitzer data, so we were not able to create any MIPS or IRAC mosaics. However, this system is covered by the WISE data, the bow shock being visible only in the WISE 22 μm channel image.

Despite the lower resolution of WISE, we are still able to extract some information from the images. The bow shock seems to be perfectly symmetric without any discernable fine structure and it has a bow-like shape. The apex of the bow shock is located at $\sim 0.3'$ which would correspond to a linear separation of $R_S \simeq 0.2$ pc from the HMXB system if we consider the given distance of 2.4 kpc.

Name	4U 1258-61
RA(J2000) [hhmmss,s]	13 01 17.1
Dec(J2000) [° ′ ″]	-61 36 07
Optical counterpart	V850 Cen
Opt. Ctp. Spectral type	B0.7Ve
J; H; K [mag]	9.798; 9.297; 9.040
distance [kpc]	2.4

Table 5.5: 4U 1258-61 general data.[5]
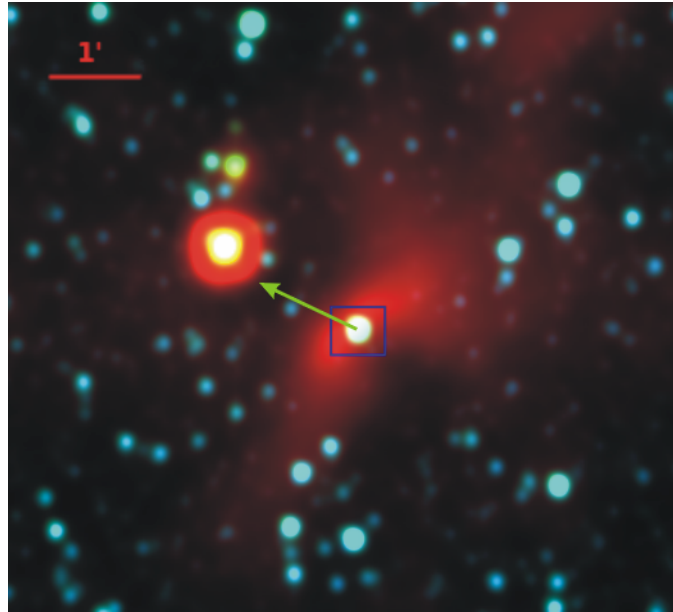

Figure 5.5: A colour image of the bow shock associated with 4U 1258-61 made from WISE data. Blue shows infrared light with wavelength of 3.4 μm (WISE ch. 1), green 4.6 μm light (WISE ch. 2) and red 22 μm light (WISE ch. 4). The HMXB is marked by the square. The arrow indicates the direction of the computed peculiar motion.

If this is indeed a stellar bow shock, this would be a first detection of a bow shock associated with a Be/X-ray binary ever. Its formation is not expected, since Be/X-ray binaries are expected to have much lower system velocities than SGXBs.

5.3.2   EXO 1722-363

EXO 1722-363 is a recently discovered heavily obscured SGXB. This system containing an X-ray pulsar is located in Galactic bulge region, a region that is difficult to study. A likely near-IR counterpart of the system is 2MASS J17251139-3616575.[50]

The system is covered by both the Spitzer and WISE data. We have detected a new bow shock around the system. Similarly to the previous two systems, the bow shock only appears in MIPS 24 μm and WISE 22 μm images.

The bow shock itself has an arcuate structure and is quite thick. The shape and structure is similar to the bow shock associated with 4U 1907+09, both being a bit asymmetric. From

Name	EXO 1722-363
RA(J2000) [hhmmss,s]	17 25 11.4
Dec(J2000) [° ′ ″]	-36 16 57.5
Infrared counterpart	2MASS J17251139-3616575 ?
Inf. Ctp. Spectral type	B0-1Ia ?
J; H; K [mag]	14.218; 11.811; 10.672
distance [kpc]	∼7

Table 5.6: EXO 1722-363 general data.[5],[48],[49],[50]

Figure 5.6 we can see that one of its wings is slightly brighter than the other. As they are no stars at this location, it is probably a feature of the bow shock itself.

The distance to the system was inferred from a typical luminosity of active accretion-powered pulsars and can be estimated as ∼7 kpc. The distance from the system to the apex of the bow shock is $\sim 0.3'$, which at the given distance would correspond to the linear separation of $R_S \simeq 0.4$ pc.
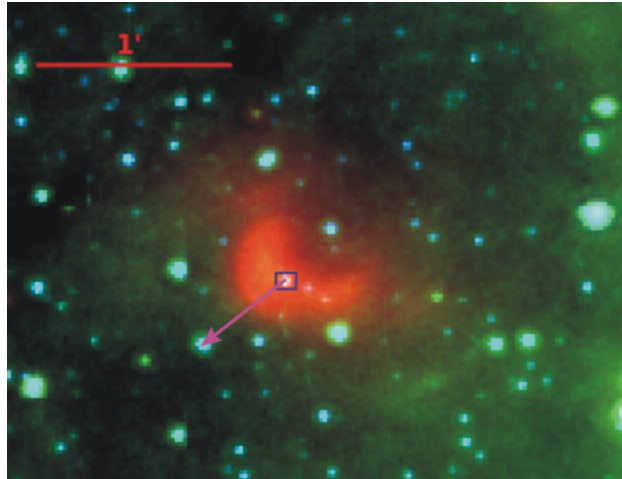
Figure 5.6: A colour image of the bow shock associated with EXO 1722-363 made from MIPS and IRAC data. Blue shows infrared light with wavelength of 3.6 μm (IRAC ch. 1), green 8.0 μm light (IRAC ch. 4) and red 24 μm light (MIPS ch. 1). The HMXB is marked by the square. The arrow indicates the direction of the computed peculiar motion.

5.4 Discussion

5.4.1 Bow shock symmetries vs proper motions

To prove that the origin of the bow shock is due to a high velocity of the system, it is a good idea to supplement our findings with proper motions measurements. Indeed, as mentioned above, the symmetry axis of a bow shock reflects the direction of the motion of the system with respect to the ambient medium, which also can be in motion relative to the local standard of rest.

The proper motions of the known bow shock producing systems, Vela X-1 and 4U 1907+09, have been previously determined. Here we use the proper motions of these two systems as given in Gvaramadze et al. (2011)[25].

To obtain the proper motion for 4U 1258-61, we searched for existing measurements for this system using the Vizier catalogue access tool[51]. We obtained the proper motions measurements from several catalogues: USNO-B1.0 ((Monet et al. 2003)[52], NOMAD (Zacharias et al. 2005)[53], PPMX (Roeser at al. 2008)[54], UCAC3 (Zacharias et al. 2010)[55] and PPMXL (Roeser at al. 2010)[56]. However, the proper motion values obtained from these catalogues deviate significantly from one another and cannot be reconciled. Thus, we had to determine the proper motion of 4U 1258-61 ourselves.

Catalogue	proper motion in RA [mas/yr]	proper motion in dec [mas/yr]
USNO-B1.0	0 ± 6	-22 ± 6
NOMAD	-2.7 ± 5	0.6 ± 5
PPMX (2008)	-11.99 ± 23.2	-32.34 ± 23.2
UCAC3	-1.5 ± 6.2	-1.8 ± 4.3
PPMXL (2010)	-6.2 ± 11.7	-12.5 ± 11.7

Table 5.7: Proper motions of 4U 1258-61 as given by various catalogues. The abbreviation mas/yr stands for milliarcsecond/year.

We collected all available image and catalogue data on 4U 1258-61. There are several catalogues giving its position and the epoch: USNO-A2 (Monet et al. 1998)[57], The HST Guide Star Catalog (Lasker et al. 1996)[58], GSC2.2 (STScI 2001)[59], USNO-B1.0 (Monet et al. 2003)[52] and PPMX (Roeser at al. 2008)[54]. To determine the position of the system on obtained image data(POSS-2, 2MASS), we used the method of finding a flux-weighted centroid in a suitable-sized aperture around the system. Using these, we measured the proper motion over a total time baseline of 24 years.
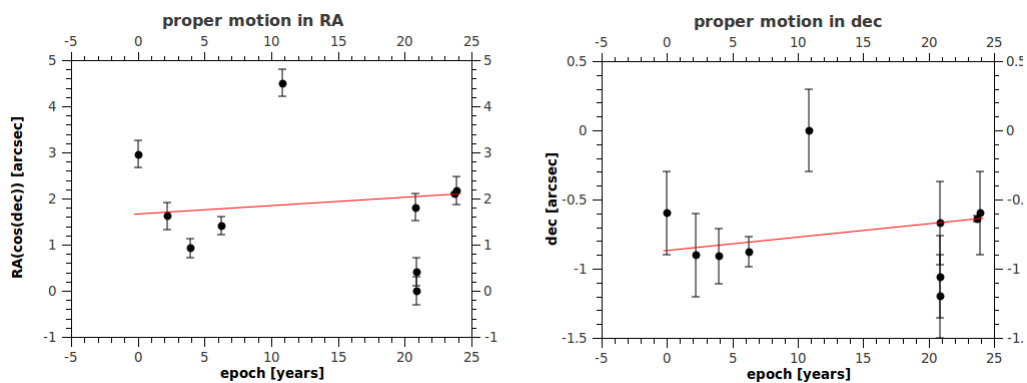

Figure 5.7: 4U 1258-61 proper motion determination via a linear fit on the positional data.

The proper motion determination of EXO 1722-363 proved to be more difficult. The system is not visible in the optical wavelengths at all, so we had to rely on 2MASS and IRAC/WISE data we worked with. The total time baseline of the measurement was only 10 years.
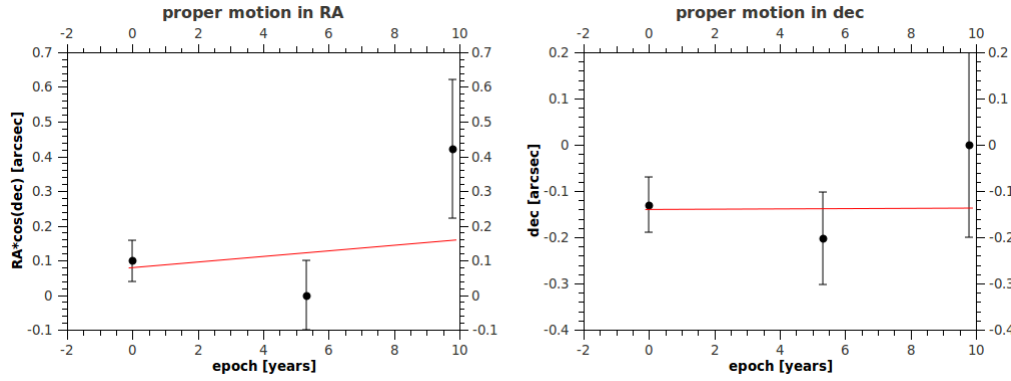
Figure 5.8: EXO 1722-363 proper motion determination via a linear fit on the positional data.

To compute the peculiar tangential velocity we used the method described in Chapter 3. We found out that all studied systems possess high tangential peculiar velocities, running away from the Galactic plane. Moreover, the directions of the computed peculiar velocities for every system fit well with the directions of velocities inferred via the bow shock axis of symmetry. This proves that the observed arcuate structures are indeed stellar bow shocks. The computed velocities can be found in Table 5.8.

	Vela X-1	4U 1907+09	4U 1258-61	EXO 1722-363
μ_α [mas/yr]	-5.48 ± 0.35	-7.7 ± 6.3	18.1 ± 5.7	8.1 ± 16.4
μ_δ [mas/yr]	8.79 ± 0.40	1.5 ± 5.3	9.7 ± 4.7	0.3 ± 16.4
μ_l [mas/yr]	-10.21 ± 0.38	-2.2 ± 5.5	18.5 ± 5.7	4.8 ± 16.4
μ_b [mas/yr]	1.68 ± 0.37	7.5 ± 6.1	9.0 ± 4.7	-6.5 ± 16.4
v_{lt} [km s^{-1}]	-91.8 ± 3.4	-41.7 ± 104.3	210.5 ± 64.8	159 ± 544
v_{bt} [km s^{-1}]	15.1 ± 3.3	142.6 ± 155.7	102.4 ± 53.5	-216 ± 544
$(v_{lt})_\odot$ [km s^{-1}]	-8.6	-1.0	-14.4	-12.4
$(v_{bt})_\odot$ [km s^{-1}]	-8.0	-7.1	-7.3	-7.3
$(v_{lt})_{rot}$ [km s^{-1}]	-52.8	-100.0	-62.6	-106
$(v_{bt})_{rot}$ [km s^{-1}]	-0.8	-0.5	0.6	-0.8
$(v_{lt})_{pec}$ [km s^{-1}]	-30.4 ± 3.4	59 ± 104	288 ± 65	277 ± 544
$(v_{bt})_{pec}$ [km s^{-1}]	24.0 ± 3.3	150 ± 116	109 ± 54	-208 ± 544
$(v_t)_{pec}$ [km s^{-1}]	38.7 ± 4.7	161 ± 156	308 ± 84	347 ± 769

Table 5.8: Tangential peculiar velocity determinations for the studied systems. The abbreviation mas/yr stands for milliarcsecond/year. For the description of the used symbols refer to Chap. 3

It should be noted that there are peculiar radial velocities measured for two of the studied systems. Vela X-1 has the peculiar radial velocity $(v_r)_{\text{pec}} = -27\,\text{km s}^{-1}$[25] and together with the peculiar tangential velocities that we calculated we can determine the peculiar velocity of the system as $v_{\text{pec}} = 47\,\text{km s}^{-1}$. The peculiar radial velocity of 4U1258-61 was determined by van Oijen (1989)[27] in a paper that used the peculiar radial velocities

to determine the percentage of runaway systems among HMXBs. Its mediocre peculiar tangential velocity of $(v_r)_{\text{pec}} = 8\,\text{km}\,\text{s}^{-1}$ was not high enough to classify the system as a runaway.

We searched for nearby OB associations which are a possible source of high-velocity outflows affecting the interstellar medium up to $80 - 100$ pc from the association.[60]. We investigated the new bow shock producing systems as they have not been previously studied.

There are several OB associations in the vicinity of 4U 1258-61: Cen A, B, C, D and E. However, according to New list of OB associations catalogue (Melnik A. M. 1995)[61] all of them lie in the foreground. We also searched for any other clusters in the radius of 2 arcdegrees (about 80 pc) around the system via Simbad[62]. However, all clusters in this radius are either foreground or background objects. Thus we conclude that there are no significant outflows from clusters or associations that may alter the geometry of the bow shock associated with 4U 1258-61.

We counducted a similar search in 100 pc radius around EXO 1722-363 for any OB associations or clusters but we were not able to find any but the foreground ones. It is not surprising given the high extinction towards the Galactic bulge meaning many clusters may avoid detection.

5.4.2   Possible parent clusters and SNRs

The calculated peculiar velocity can be used to back-trace the motion of the system. Using such a method, the parent cluster or association can be determined. It may be also possible to determine a supernova remnant (SNR) that might be associated with the system.

Using this method, Kaper et al. (1997)[46] determined the OB association VelOB1 (distance 1.82 pc) as a possible 'birth site' of Vela X-1. This method was employed by Gvaramadze et al. (2011)[25] as well, but they were not able to find any cluster, association or a supernova remnant that might be associated with 4U 1907+09.

We also attempted to exploit this method for the newly discovered systems with bow shocks. If we assume that HMXBs are formed near the Galactic plane, we can trace back the motion inferred from the peculiar velocity until it intersects the plane ($b = 0°$). This area may be considered as a likely formation site of the system ($l = 300.9°, b = 0°$ for 4U 1258-61 and $l = 350.8°, b = 0°$ for EXO 1722-363). It is also possible that the parent cluster or SNR might be located in the area between the 'birth site' and the present location of the system.

To search for any possible related SNRs we used Chandra Catalog of Galactic Supernova Remnants[63] and revised Galactic supernova remnant catalogue (Green at al. 2009)[64]. We found a supernova remnant G302.3+0.7 that may be related to 4U 1258-61 at $l = 302.3°, b = 0.7°$. If we assume that the system is connected to the SNR, we are able to estimate its kinematical age (e.g. how much time has elapsed since the supernova explosion). Using the peculiar velocity of the system, we estimate $t_{\text{kin}} = 2.2 \times 10^5$ yr which is well within the expected lifetime of SNRs $t_{\text{lif}} = 5 \times 10^5$ yr as given by Shull et al. (1989)[60]. However, Kaspi et al (1996)[65] estimate the distance of the SNR $d = 8$ kpc. Thus the remnant is probably not associated with the HMXB. We also searched for SNRs that might be associated with EXO 1722-363, but there are no catalogued SNRs in

the vicinity of the system.

The search for parent clusters or associations also yielded inconclusive results. We used Simbad[62] and New list of OB associations catalogue (Melnik A. M. 1995)[61] to look for any clusters and associations that might be connected to the two studied HMXB systems. There are several clusters present at the probable location of formation of 4U 1258-61, however they are either in the background (Hogg 15, [DBS 2003] 78) or in the foreground (NGC 4609). As the system possesses only a small peculiar radial velocity it is unlikely that it is associated with any of these. There are several clusters recently detected by the GLIMPSE survey ([MCM2005b] 32 and 33) but their distance is not precisely determined (median distance for such objects may be approximately 3 kpc)[66], so whether they are related to 4U 1258-61 or not is questionable. No possible parent OB associations were found. There are many clusters in the zone of formation of EXO 1722-363 as well, but they are associated with NGC 3634, which lies only 1.7 kpc away. Similarly to the previous case, no parent OB associations that lie at the expected position and distance were found.

Our inability to determine the parent clusters or associations is not surprising. One possible cause might be due to high extinction. Another plausible scenario is that the binary system was expeled from ist parent cluster or association prior to the supernova explosion of one of its members. The supernova explosion may have propelled the system away from its initial course, so the determination of the parent cluster via the used method may produce no results.

5.4.3 Number density of the medium estimate

Determining the stand-off distance of the shock and the peculiar velocity of the system enable us to make an estimate of the number density of the ambient medium (provided that we know the mass-loss rates and stellar wind velocity of the system). For Vela X-1 and 4U 1907+09 we adopted the mass-loss rates from Gvaramadze et al. (2011)[25] and for EXO 1722-363 we adopted the values given by Manousakis & Walter (2010)[67]. We were not able to find the mass-loss rates and wind velocity for 4U 1258-61. Instead, we adopt the values for π Aqr, which is a Be star with similar parameters to the optical counterpart of 4U 1258-61 (the spectral type of π Aqr is B1Ve, the optical counterpart of 4U 1258-61 is B0.7Ve) as given by Snow (1981)[68]. The number density can be calculated from Eq. (3.7) or, as in [25], one may rewrite the equation as:

$$n = 0.5 \, \text{cm}^{-3} \left(\frac{\dot{M}}{10^{-6} \text{M}_\odot \, \text{yr}^{-1}} \right) \left(\frac{v_w}{2000 \, \text{km s}^{-1}} \right) \left(\frac{R_S}{1 \, \text{pc}} \right)^{-2} \left(\frac{v_\star}{100 \, \text{km s}^{-1}} \right)^{-2}. \quad (5.1)$$

It would appear that Vela X-1 is moving through denser medium than all other systems despite the fact that it is located the furthest from the galactic plane from all the studied systems. On the other hand, 4U 1258-61 and EXO 1722-363 move throught the medium that is relatively rarified. These computed values are only estimates at best, as we do not have the precise mass-loss rates and wind velocity for 4U 1258-61, and the peculiar velocity of EXO 1722-363 suffers from large errors.

HMXB	v_w	$\dot{M}$	R_S	$v_\star$	n
	[km s^{-1}]	[10^{-6} M$_\odot$ yr^{-1}]	[pc]	[km s^{-1}]	[cm^{-3}]
Vela X-1	1100	2	0.5	47	9
4U 1907+09	1690	6	0.8	161	1.5
4U 1258-61	1450	0.0026	0.2	308	0.0025
EXO 1722-363	400	1.5	0.4	347	0.08

Table 5.9: Number density of the ambient medium estimates ($v_\star = v_{pec}$).

5.4.4 Vela X-1 bow shock spectrum
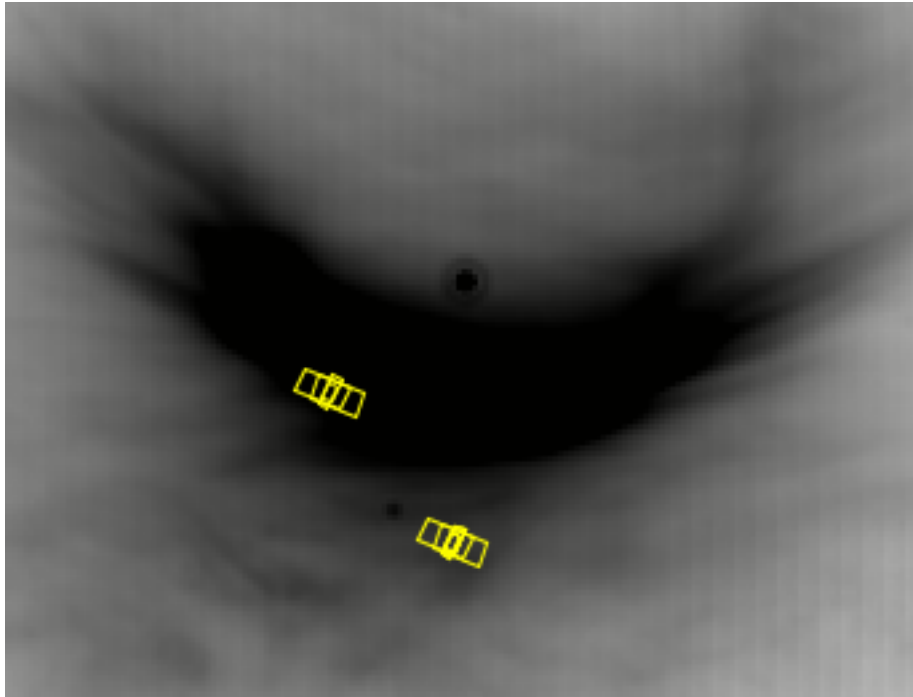
Figure 5.9: IRS target and background slits positions overlaid on a MIPS 24 μm mosaic of Vela X-1.

We have obtained a spectrum of Vela X-1 bow shock from the slit position indicated in Figure 5.9. The spectrum is dominated by a continuum emission that starts to rapidly increase from 14 μm to the longer wavelengths. There are about a dozen prominent emision lines present in the spectrum, but we were able to identify only half of them (Ne V, Cl II, S III – two lines, Ne III and possibly S(0) rotational H$_2$ line, see Table 5.10). For the other half of them we were not able to find any possible match in the line list given in Glass (1999)[69]. The other emission features might be artifacts.

During the closer inspection of the background slit position overlaid on MIPS and IRAC mosaic we found out that there is a patch of nebulosity contaminating the background spectrum. This may adversely influence the shape of the continuum and the line intensities as well. The inspection of the spectrum without subtracting the background may be possible to some degree, but without the background spectrum we would not be able to
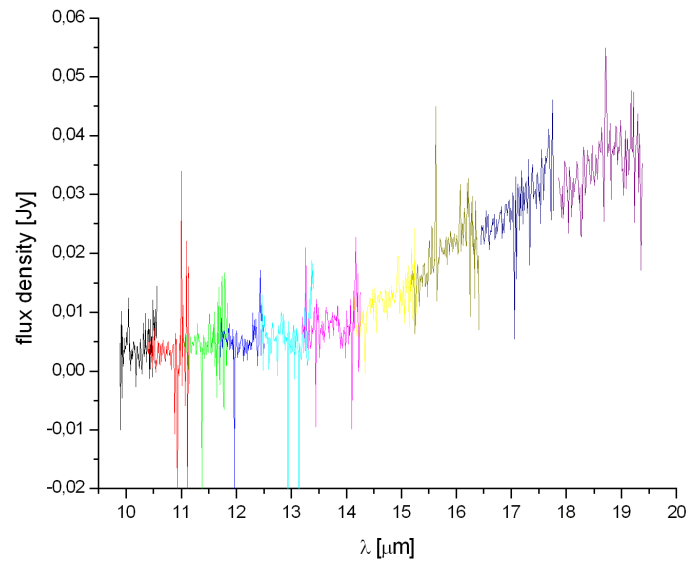
Figure 5.10: Vela X-1 bow shock spectrum (short wavelengths). Spectral orders are distinguished by colour.
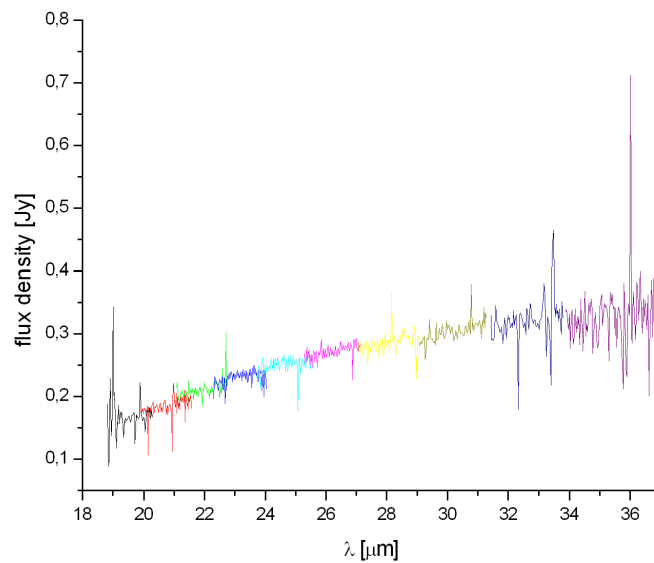

Figure 5.11: Vela X-1 bow shock spectrum (long wavelengths). Spectral orders are distinguished by colour.

mitigate most of the artifacts that would otherwise be present in the spectrum. Considering these facts, we did not attempt further investigation of the shock via the spectrum, leaving it as an avenue for a further study.

spec. line	λ_{cat} [μm]	λ_{obs} [μm]	flux density [Jy]
Ne V	14.322	14.32	0.027
Cl II	14.368	14.37	0.016
S III	18.713	18.71	0.055
S III	33.481	33.48	0.464
Ne III	36.014	36.01	0.729
S (0)	28.22	28.17	0.368

Table 5.10: Emission features present in the spectrum.

5.4.5   Paucity of bow shocks around HMXBs

Huthoff & Kaper (2002)[30] hypothesize about the difference in occurence of bow shocks associated with HMXBs and OB runaway stars. They argue that OB runaways have been expelled from their parent association at a relatively early stage, when the cluster was still very dense and the probability of close encounter leading to ejection of the star from the association was high. On the other hand, OB stars in HMXB systems went through several stages of binary evolution before becoming runaways after the occurence of a supernova explosion within the system. Therefore, the kinematical age of HMXB systems should be smaller than the kinematical age of most OB runaways. Thus, HMXBs have a higher probability to be still enclosed in the hot and rarefied regions (superbubles) that surround OB associations.

In their sample consising of 11 HMXBs, they were able to detect only one bow shock but given the poor detection sensitivity of IRAS beyond 2kpc, they were left with only one system out of five that produces bow shock (In later work, Gvaramadze et al. (2011)[25] using the same sample of 11 HMXBs detected one more bow shock around one of them, but then the bow shock detection rate is still around 20 %). They suggested that the comparison of HMXB bow shock detection rate to the detection rate of bow shocks around OB runaways (which is about 40 % [30]) may support this hypothesis. However, their sample was too small to produce any statistically significant results, so they were not able to support their reasoning.

Our bow shock survey gives us the opportunity to investigate this. Doing the simple math, the bow occurence around the studied HMXBs is only about 3 %. Given the higher sensitivity of the Spitzer and WISE, and our sample of 118 HMXBs we conclude that the hypothesis above is plausible.

Chapter 6

Conclusion

In this work we have studied High Mass X-ray binaries (HMXBs) with associated stellar bow shocks. In Chap. 1 we introduced X-ray binaries and pointed out plethora of their interesting aspects that might motivate us to study them. Chap. 2 focuses more on one of the classes of X-ray binaries, HMXBs, that are studied in this thesis. Further on, in Chap. 3 we provide a short introduction to stellar bow shock physics, which enable us to investigate the velocity of the HMXB system, the stellar wind and properties of the surrounding interstellar medium. We then discuss HMXBs as runaway objects and origins of their high space (peculiar) velocities. Next, we provide a short overview of HMXB investigations via bow shocks and a short section about the peculiar velocity determination.

Chap 4. starts the practical part of the thesis. Here we discuss the space missions and instruments aboard from which we obtained the data. We have focused heavily on the topic of data reduction. Finally, in Chap. 5, we present our bow shock survey and our findings.

In total, we found four systems with observable bow shocks, two of them: Vela X-1 and 4U 1907+09 are known and have been studied previously. We report a discovery of two new bow shock candidates around HMXB systems: 4U 1258-61 and EXO 1722-363, with the evidence suggesting that the are very likely genuine stellar bow shocks.

Via the orientations of the bow shock axis of symmetry associated with the HMXBs and peculiar velocities calculated from the proper motions of the systems, we conclude that all four studied HMXBs are runaway systems possessing high peculiar velocities. The directions of motion for the studied HMXBs inferred from the bow shock geometry and from the peculiar velocity correspond well in all the cases (despite the large error bars). The direction of their respective motions suggests that they are running away from the Galactic plane.

The occurence of a bow shock in vicinity 4U 1258-61, is particulary surprising. It is a first bow shock found around a Be/X-ray binary. These types of X-ray systems are not expected to form bow shocks because of their low peculiar velocities resulting from the supernova explosion. Its high peculiar velocity of more than $300 \, \mathrm{km \, s^{-1}}$, a lot higher that that of Vela X-1 and 4U 1907+09, is challenging to explain and should be a subject of further investigation.

The search for parent clusters/associations and associated supernova remnants of the new bow shock-producing systems yielded no conclusive results. It may be due to the

high extinction or, the other acceptable explanation is that the systems were expelled from the association prior to one of its component's supernova explosion which would propel the system in a new direction.

Using the velocities of the stellar wind and mass loss rates from other sources and the stand-off distance of the bow shocks measured from our images of the systems, we were able to calculate the estimates of the number density of the surrounding ambient medium around the studied HMXBs. Surprisingly, Vela X-1 moves through the densest medium despite the fact that it is located the furthest from the Galactic plane out of all the systems.

We also provide a spectrum of Vela X-1 bow shock, showing a continuum emission and a few emission spectral lines but we do not attempt any further analysis in this work mainly because of the artifacts present and the nebulosity feature contaminating the background spectrum.

Finally, we support the hypothesis of Huthoff & Kaper (2002)[30] about the discrepancy in occurence of bow shocks around OB runaways and HMXBs. It would indeed appear that the kinematical ages of most HMXBs are lower than the kinematical ages of most OB runaways. This means that most HMXBs are still moving in the superbubble created by their parent OB association, not producing bow shocks despite their runaway velocities. This is consistent with the results of our HMXB bow shock survey, with the bow shock detection rate of only 3 % as compared to the 40 % bow shock occurence around OB runaways.

Bibliography

[1] Giaconni, R., Gursky, H., Paolini, F. Rossi, B. 1962 Phys. Rev. Lett. **9**, 439.

[2] Zel'Dovich, Ya. B., Guseinov, O. Kh., SvA, **10**, 251 (1966).

[3] Shklovsky, I. S.: *On the Nature of the Source of X-Ray Emission of SCO XR-1*, ApJ, **148**, p.L1.

[4] Prendergast, K. H., Burbidge, G. R.: *On the Nature of Some Galactic X-Ray Sources*, ApJ, **151**, p.L83.

[5] Liu, Q. Z., van Paradijs, J., van den Heuvel, E. P. J.: *Catalogue of high-mass X-ray binaries in the Galaxy (4th edition)*, A&A **455**, 1165–1168 (2006).

[6] Biswajit, P., Sachindra, N.: *Transient High Mass X-ray Binaries*, Bull. Astr. Soc. India, **39**, 1.

[7] http://www.phy.ohiou.edu/~mboett/gbhc.html.

[8] Lewin, H. G. W., van der Klis, M.: *Compact Stellar X-ray Sources*, Cambridge University Press, Cambridge, 2006.

[9] Padmanbhan, T.: *Theoretical Astrophysics - volume II: Stars and Stellar systems*, Cambridge University Press, Cambridge, 2001.

[10] http://pulsar.sternwarte.uni-erlangen.de/wilms/teach/xrb/index.html.

[11] Meurs, E. J. A., van den Heuvel, E. P. J., A&A, **226**, 88 (1966).

[12] Camenzind, M.: *Compact Objects in Astrophysics, White Dwarfs, Neutron Stars and Black Holes*, Springer, Berlin, 2007.

[13] Knigge, C., Coe, M. J., Podsiadlowski, P.: *Two populations of X-ray pulsars produced by two types of supernova*, Nature, **479**, 372.

[14] Reig, P.: *Be/X-ray binaries*, Astrophys. Space Sci., **332**, 1-29.

[15] Naik, S., Blesson, M., Banerjee, D. P. K., et al.: *Near-infrared Observations of Be/X-ray Binary Pulsar A0535+262*, Res A&A, **12**, 177.

[16] Blondin, J. M., Stevens, I. R., Kallman, T. R., ApJ, **371**, 684 (1991).

[17] Chaty, S.: *High Energy Phenomena in Supergiant X-ray Binaries*, arXiv:1005.1995v1 [astro-ph.HE].

[18] Pfahl, E., Rappaport, S., Podsiadlowski, P., Spruit, H., ApJ, **574**, 364 (2002).

[19] Podsiadlowski, P., Pfahl, E., Rappaport, S.: *Neutron-Star Birth Kicks*, Binary Radio Pulsars, ASP Conference Series, **328**, 327.

[20] Chaty, S.: *Multi-wavelength study of High Mass X-ray Binaries*, arXiv:1008.2718v1 [astro-ph.HE] (2010).

[21] Mirabel, I. F.: *Gamma-ray binaries revealed*, Science, **335**, 175 (2012).

[22] The Fermi LAT collaboration: *Periodic emission from the Gamma-ray Binary 1FGL J1018.6-5856*, Science, **335**, 189 (2012).

[23] Sparavigna, A. C., Marazzato, R.: *Observing stellar bow shocks*, arXiv:1005.1527v1 [physics.space-ph].

[24] http://casa.colorado.edu/~danforth/science/shocks/index.html.

[25] Gvaramadze, V. V., et al.: *4U 1907+09: a HMXB running away from the Galactic plane*, arXiv:1102.2437v1 [astro-ph.SR].

[26] Kobulnicky, H. A, Gilbert, I. J., Kiminky, D. C.: *OB Stars & Stellar Bow-shocks in Cygnus-X: A Novel Laboratory Estimating Stellar Mass Loss Rates*, arXiv:0912.1314v1 [astro-ph.GA].

[27] van Oijen, J. G. J.: *Are massive X-ray binaries runaway stars?*, A&A, **217**, 115-126 (1989).

[28] Kaper, L.: *High-mass X-ray binaries and OB-runaway stars*, arXiv:astro-ph/0101303v1.

[29] Peri, C. S., et al.: *E-BOSS: an Extensive stellar BOw Shock Survey. I: Methods and First Catalogue*, arXiv:1109.3689v2 [astro-ph.SR].

[30] Huthoff, F., Kaper, L.: *On the absence of wind bow-shocks around OB-runaway stars: Probing the physical conditions of the interstellar medium*, A&A, **383**, 999-1010 (2002).

[31] Mdzinarishvili, T. G., Chargeishvili, K. B.: *New runaway OB stars with HIPPARCOS*, A&A, **431**, L1- L4 (2005).

[32] Clemens, D. P., ApJ, **295**, 422 (1985).

[33] Fazio, G. G., et al., ApJS, **154**, 10 (2004).

[34] Houck, J. R., et al., ApJS **154**, 18 (2004).

[35] Rieke, G. H., et al., ApJS, **154**, 25 (2004).

[36] http://irsa.ipac.caltech.edu/data/SPITZER/docs/spitzermission/missionoverview/spitzertelescopehandbook/.

[37] http://irsa.ipac.caltech.edu/data/SPITZER/docs/mips/mipsinstrumenthandbook/.

[38] http://irsa.ipac.caltech.edu/data/SPITZER/docs/dataanalysistools/cookbook/.

[39] http://irsa.ipac.caltech.edu/data/SPITZER/docs/dataanalysistools/tools/mopex/mopexusersguide/.

[40] http://irsa.ipac.caltech.edu/data/SPITZER/docs/irac/iracinstrumenthandbook/.

[41] http://irsa.ipac.caltech.edu/data/SPITZER/docs/irs/irsinstrumenthandbook/.

[42] http://irsa.ipac.caltech.edu/data/SPITZER/docs/dataanalysistools/tools/spice/spiceusersguide/.

[43] Wright, E. L., et al.: *The Wide-field Infrared Survey Explorer (WISE): Mission Description and Initial On-orbit Performance*, arXiv:1008.0031v2 [astro-ph.IM].

[44] http://wise2.ipac.caltech.edu/docs/release/prelim/expsup/sec2_3f.html.

[45] Kreykenbohm, I., et al.: *Highly structured wind in Vela X-1*, arXiv:0903.0838v1 [astro-ph.HE].

[46] Kaper, L., et al.: *Discovery of a Bow Shock around Vela X-1*, ApJ, **475**, L37 (1997).

[47] Devasia, J.: *Timing and spectral studies of the transient X-ray pulsar GX 304-1 during an outburst*, arXiv:1106.3251.

[48] http://simbad.u-strasbg.fr/simbad/sim-id?Ident=IGR%20J17252-3616.

[49] http://simbad.u-strasbg.fr/simbad/sim-id?Ident=2MASS%20J17251139-3616575.

[50] Zurita Heras, J. A., et al.: *IGR J17252-3616: an accreting pulsar observed by INTEGRAL and XMM-Newton*, arXiv:astro-ph/0511115v1.

[51] http://vizier.u-strasbg.fr/viz-bin/VizieR.

[52] Monet, D. G., Levine, S.E., Casian, B., et al, AJ, **125**, 984 (2003).

[53] Zacharias, N., Monet, D. G., Levine, S. E.: *Naval Observatory Merged Astrometric Dataset (NOMAD)*, San Diego AAS Meeting, January 2005.

[54] Roeser, S., Schilbach, E., Schwan, H., et al, A&A, **488**, 201 (2008).

[55] Zacharias, N., Finch, C., Girard, T., et al., AJ, **139**, 2184 (2010).

[56] Roeser, S., Demleitner, M., Schilbach, E., AJ, **139**, 2440 (2010).

[57] Monet, D. G., Canzian, B., Dahn, C., et al.: *USNO-A V2.0, A Catalog of Astrometric Standards*, USNOFS & USRA (1998).

[58] Morrison J. E., Roeser S., McLean B., et al.: *The Guide Star Catalog Version 1.2: an astrometric recalibration and other refinements*, AJ, **121**, 1752 (2001).

[59] The Guide Star Catalogue (Version 2.2.01), STScI & Osservatorio Astronomico di Torino (2001).

[60] Shull, J. M., Fesen, R. A., Saken, J. M., ApJ, 346, 860 (1989).

[61] Melnik A. M., Efremov Yu. N.: *New list of OB associations of our Galaxy*, Pis'ma Astron. Zh, **21**, 13 (1995).

[62] http://simbad.u-strasbg.fr/simbad/.

[63] http://hea-www.cfa.harvard.edu/ChandraSNR/snrcat_gal.html.

[64] Green, D. A., Bulletin of the Astronomical Society of India, **37**, 45 (2009).

[65] Kaspi, V. M., Manchester, R. N., Johnston, S., et al.: *A Search for Radio Pulsars in Southern Supernova Remnants*, AJ, **111**, 2028 (1996).

[66] Mercer, E. P., Clemens, D. P., Meade, M. R., et al.: *New Star Clusters Discovered in the GLIMPSE Survey*, AJ, **635**, 560 (2005).

[67] Manousakis, A., Walter, R.: *X-ray Wind Tomography of the highly absorbed HMXB IGR J17252-3616*, arXiv:1008.5362v1 [astro-ph.HE].

[68] Snow, T. P., Jr.: *Stellar winds and mass-loss rates from Be stars*, AJ, **251**, 139 (1981).

[69] Glass, I. S.: *Hanbook of Infrared Astronomy*, Cambridge University Press, Cambridge, 1999.